The Thesis Committee for Prashant Alok
Certifies that this is the approved version of the following Thesis:

APPLICATION OF ADDITIVELY MANUFACTURED CONFORMAL NEGATIVE STIFFNESS HONEYCOMBS FOR IMPACT ISOLATION IN PROTECTIVE HEADGEAR

APPROVED BY
SUPERVISING COMMITTEE:

Carolyn C. Seepersad, Supervisor

Michael R. Haberman

APPLICATION OF ADDITIVELY MANUFACTURED CONFORMAL NEGATIVE STIFFNESS HONEYCOMBS FOR IMPACT ISOLATION IN PROTECTIVE HEADGEAR

By

Prashant Alok

Thesis

Presented to the Faculty of the Graduate School of

The University of Texas at Austin

in Partial Fulfillment

of the Requirements

for the Degree of

Master of Science in Engineering

The University of Texas at Austin

August 2018

Acknowledgements

At the outset, I would like to express my utmost gratitude for the constant help, support and guidance provide by my graduate advisor, Dr. Carolyn. C. Seepersad. I am extremely grateful to her for the countless review meetings and key suggestions during the entire course of this research. I really appreciate the time she took out from her busy schedule to help me out and am honored to have worked under her supervision. This opportunity has been a great learning experience through and through which has made me a better student and a better person than when I started. I am also grateful to her for providing financial support for my research time and again. I would also like to express my gratitude to Dr. Michael R. Haberman for his time and valuable feedback on this research. I am also thankful to the University of Texas at Austin and the faculty members for their guidance and for sharing their knowledge with me.

I would also like to thank my family for their unconditional love and support. It would not have been possible without them.

I would like to acknowledge the help of David Debeau for his help with this research. I am also thankful to my colleagues and lab mates - Ademola Oridate, Clint Morris, Conner Sharpe, Jared Allison, Oliver Uitz, and Tyler Wiest at the PPMD lab here at the University of Texas at Austin. I am also thankful to my friends Devashri Khadke, Krishna Murthy, and Sridharan Vasu for their constant support and encouragement.

Abstract

APPLICATION OF ADDITIVELY MANUFACTURED CONFORMAL NEGATIVE STIFFNESS HONEYCOMBS FOR IMPACT ISOLATION IN PROTECTIVE HEADGEAR

Prashant Alok, M.S.E

The University of Texas at Austin, 2018

Supervisor: Carolyn C. Seepersad

The primary goal of this research is to study the implementation of conformal negatives stiffness elements for impact isolation in baseball helmets. These conformal elements utilize pre-curved beams designed to a specific geometric profile that have been exhibited to have better impact absorption due to their snap-through behavior. A preliminary study is carried out to develop a thorough understanding of pre-curved beams and the negative stiffness elements that utilize this concept. The basic principles and equations of such structures are discussed. Subsequently, the application of the above principles in the context of conformal negative stiffness design is studied. A conformal negative stiffness element is designed and manufactured by SLS using nylon 11. Preliminary tests done on these elements indicated a requirement to improve the effectiveness of the elements so that they are able to absorb impacts of low as well as high magnitude. A novel method to increase the effectiveness by introducing variable force thresholds in these elements is introduced and discussed. The methodology for designing and optimizing an improved element is discussed. The elements are manufactured by SLS

using nylon 11. FEA analysis of these elements are carried out in ABAQUS under quasi-static conditions and dynamic conditions. The elements are subjected to physical quasi-static and impact testing as well. Finally, the performance of these elements is compared to a conventional padding used in baseball helmets under one-dimensional impacts using a drop test rig. The results obtained from physical tests are also compared with those obtained from FEA analysis.

Table of Contents

List of Tables

List of Figures

Chapter 1: Introduction

1.1 MOTIVATION

Baseball is an extremely popular sport in the United States with approximately 19 million people participating in the sport, out of which 5 million are children under the age of 14 (Viano *et al*., 1993). Moreover, there are approximately 400,000 high school and 20,000 collegiate baseball athletes in the Unites States (Rutherford *et al.,* 1984). As is common with many sports, various injuries are associated with baseball. The most common mode of injury in baseball is due to ball-player impact, which accounts for approximately 52%-62% of the total injuries (Gessel *et al*., 2007). Some of the most severe injuries are associated with direct impact of a baseball on a helmet leading to concussions and in some cases, fatalities. Also, the number of injuries is likely to be under reported because it does not take into account injuries treated by family doctors or other medical professionals (McRea *et al.*, 2004). Studies related to these injuries have shown that reported concussions occur at a rate of 0.08 per 1000 athlete exposures (exposure refers to the athlete's participation in a game or practice) at the high school level and 0.23 per 1000 athlete exposures at the collegiate level of competitive baseball games (Gessel *et al*., 2007). Nearly 51% of ball-player injuries are a result of helmet hit-by-pitch (H-HBP) impacts (Gessel *et al*., 2007).

The standard protective head gear used by baseball batters is a helmet. The helmets available in the market are rated and validated against National Operating Committee on Standards for Athletic Equipment (NOCSAE) standards, which prescribe an impact velocity of 60 mph ± 3%. However, at competitive level the pitches are thrown well above this prescribed velocity. Also, although the NOCSAE standards specify various locations on the helmet where the baseball/softball impact should be measured, they do not analyze

the effect of repeated impacts on the helmet. Most of the shock absorbing elements lining the helmet undergo plastic deformation on the first impact even though there might be no apparent observable deformity to the helmet shell. It not only renders the helmet less effective at mitigating impacts, but also since there might be no observable deformity, the helmet may be used by the batter again, compromising his/her safety even for a second impact of lower magnitude.

The pitchers are also at risk of getting injured when they are in the path of line drives or other hits in their direction. The average exit velocity of a baseball after being hit is upwards of 85 mph and may be as high as 120 mph (Baseball Savant website). Hence, there is a need for designing shock absorbing structures that provide better impact isolation for impacts of greater magnitude as well as for repeated impacts.

Extensive research has been done to understand the correlation between concussion and impact magnitude. Work done by Rowson and Duma at Virginia Tech has sought to correlate the head impact exposure and the risk of concussion in football players. They analyzed 62,974 head acceleration data points and formulated an injury risk function. As is shown in Figure 1.1, sub concussive impacts exhibit an average head acceleration of 26±20g (median of 19g) while concussive impacts exhibit an average acceleration of 105±27g (median of 103g).

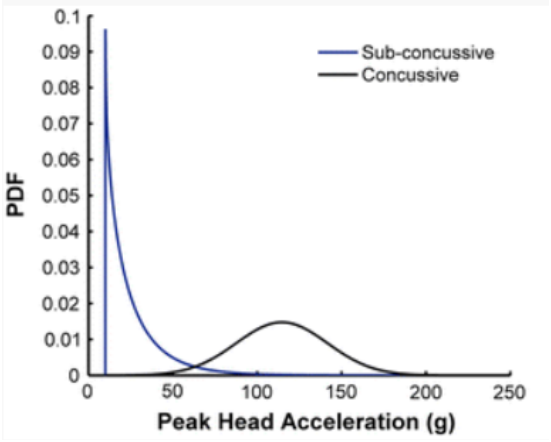

Figure 1.1: Weibull probability density function for all sub-concussive impacts and normal probability function for all concussive impacts. (Rowson and Duma, 2011)

The aim of the research is to develop an impact isolation padding to reduce the risk of mild traumatic brain injuries or m-TBI in baseball players. As much as the batters are at risk of sustaining head injuries, the pitchers are also at a risk of sustaining severe impacts to their head as a result of line drives. The research work focuses on using negative stiffness structures for developing a protective padding that can be used in helmets or caps.

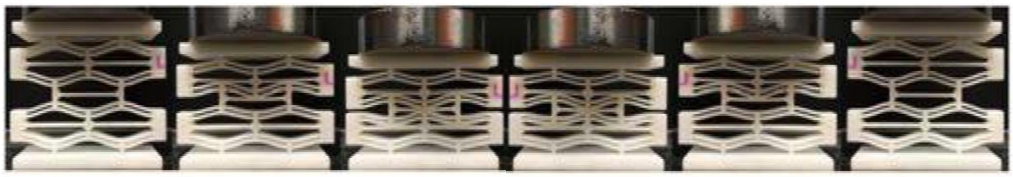

Figure 1.2: A SLS NS honeycomb prototype through various stages of compression. (Correa *et al.*, 2015)

Figure 1.2 shows a prototype of a NS honeycomb structure. These negative stiffness structures utilize curved beams designed to a specific geometric profile. As these curved beams deform they exhibit a positive force-displacement slope up to a certain force

threshold after which they snap through to a symmetric buckled position, assisting the applied force as it deforms the structure (Figure 1.3).

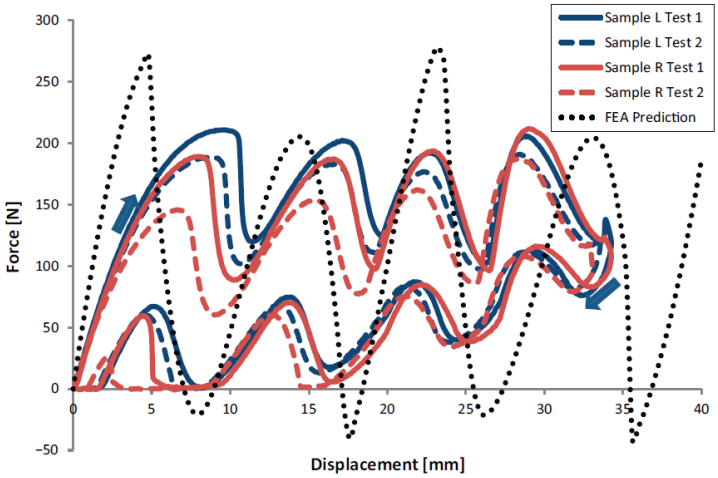

Figure 1.3: Force displacement curve of the NS honeycomb structure shown in Figure 1.2. (Correa *et al.*, 2015)

The desirable force threshold can be achieved by varying the design parameters of the pre-curved beams. In response to shock or a high magnitude of force the beams snap through after the force threshold is reached and displace even as the response force remains constant. This effect helps in providing better energy absorption. Furthermore, the design parameters of these structures can be defined such that once the external force is removed, the elements regain their original shape and hence can be reused.

1.2 Previous Work

Significant prior research has focused on developing novel methods for impact isolation. One of the traditional ways has been to develop honeycomb structures consisting of repeated unit cells or lattice structures. The traditional honeycomb structures have shown

good impact isolation behavior; however, they undergo plastic deformation after an impact and cannot be re-used. Hence, there is a need for developing unit cells or lattice structures that can recover after an impact such that the honeycombs can be used again and again. One of the methods for recovery after shock is to modify the micro lattices of such structures. Ultra-light materials based on hollow tube metallic micro lattices have been developed which have exhibited complete recovery even after excessive deformation (Schaedler *et al*., 2011), but their force thresholds are typically quite low.

Repetitive negative stiffness elements have also been used for vibration isolation and impact mitigation. One of the most common ways to implement negative stiffness is through buckled beams. Buckled beams can be created by applying equal axial loads on both ends of the beam.

Figure 1.4: Buckled beam with axial load.

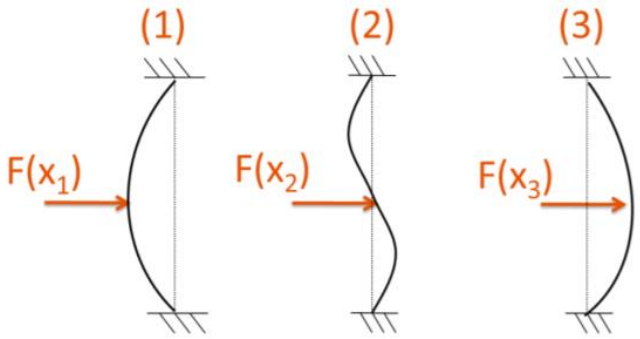

Figure 1.5: Stable and meta-stable states of a buckled beam. (Fulcher *et al.,* 2014)

Pre-buckled beams have been shown to exhibit bi-stability. The states (1) and (3) shown in Figure 1.5 correspond to the two equilibrium positions while (2) is the meta stable equilibrium state where the beam moves to either (1) or (3) even for an extremely small change in force(Fulcher *et al.,* 2014).The force versus displacement characteristic corresponding to these states is shown in Figure 1.6.

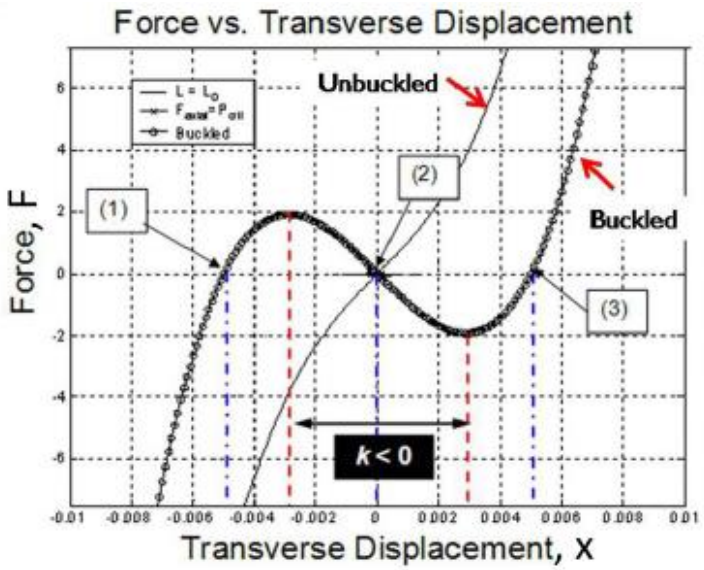

Figure 1.6: Force versus displacement behavior of a buckled beam. (Fulcher *et al.,* 2014)

For our application mono-stability is the key to ensure recovery of the structure after the impact, such that the negative stiffness element possesses only one stable equilibrium position (i.e., it snaps through upon impact and then snaps back on its own). Kashdan *et al.,* (2009) and Fulcher *et al.,* (2014) further investigated the application of buckled beams and achieved mono-stability by using a linear spring in conjunction with the buckled beams.

Qiu *et al*., (2004) in order to reduce the residual compressive stress in the buckled beams discussed above, investigated the use of pre-curved beams to achieve negative stiffness properties. They formulated a set of analytical equations for the shape of the pre-curved beams and the force-displacement relationships for the beams as a function of various design parameters.

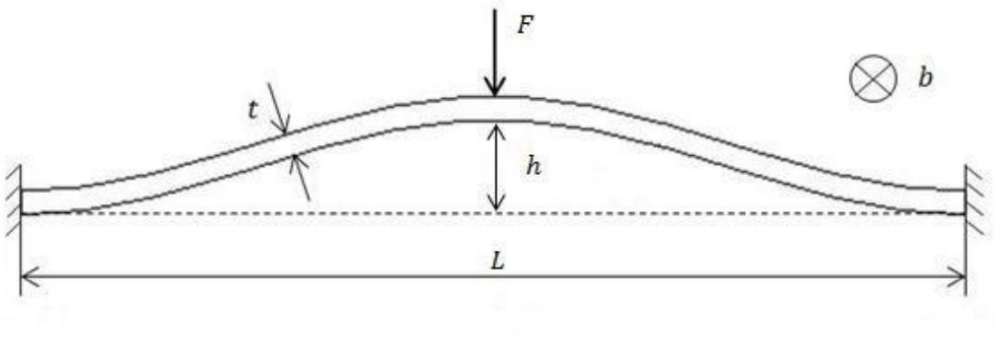

Figure 1.7: Pre-curved beam (Qiu et al., 2004)

The equation governing the geometry of the beam is as below:

$$\bar{w} = \frac{h}{2}[1 - cos\left(2\pi\frac{x}{L}\right)] \qquad (1.1)$$

where, L is the length of the beam, x is the distance from the left end of the beam, h is the maximum height of the beam and $\bar{w}$ is the corresponding transverse height of the beam at a distance x.

Qiu *et al*., (2004) also defined a factor, Q, which is indicative of the behavior of the beam. The beams were found to be mono or bi-stable with negative stiffness characteristics for a certain range of Q values.

$$Q = \frac{h}{t} \qquad (1.2)$$

where, h is the maximum height of the beam, and t is the thickness of the beam. Qiu *et al.,* (2004) also formulated an expression relating normalized force to normalized displacement Δ, equal to x/h, as follows:

$$F = \frac{3\pi^4 Q^2}{2}\Delta\left(\Delta - \frac{3}{2} + \sqrt{\frac{1}{4} - \frac{4}{3Q^2}}\right)\left(\Delta - \frac{3}{2} - \sqrt{\frac{1}{4} - \frac{4}{3Q^2}}\right) \qquad (1.3)$$

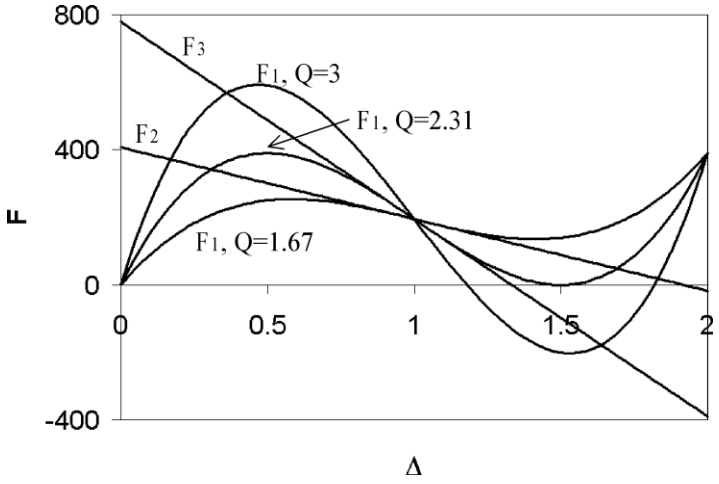

Figure 1.8: Force displacement relations of pre-curved beams for different Q values (Qiu et al., 2004)

Figure 1.8 exhibits the normalized force F_1 versus normalized displacement curve obtained using equation 1.3. Qiu *et al*., (2004) found out in their experiments that bi-stability could be achieved for Q>2.31. Further, keeping the length and thickness constant, the force threshold for the beams to snap through could be increased by increasing the Q factor. Klatt *et al.,* (2013) further expanded on this research and found that for Q = 1, the beams exhibited strictly positive stiffness, for Q values closer to 1.2, almost flat force-displacement curves were obtained indicating quasi-zero stiffness, and the beams exhibited negative stiffness with mono-stability up to Q < 2.31. For Q > 2.31, the beam was found to be bi-stable. Negative stiffness behavior along with mono-stability is extremely desirable for our application

Using the pre-curved beam geometry prescribed by Qiu *et al*., (2004) Correa *et al.,* (2015) devised a novel method to use pre-curved beams and constrain the second mode buckling to form negative stiffness honeycomb structures as shown in Figure 1.9. These structures were extensively analyzed and found to successfully recover their original geometry and force-displacement behavior even after repeated impacts.

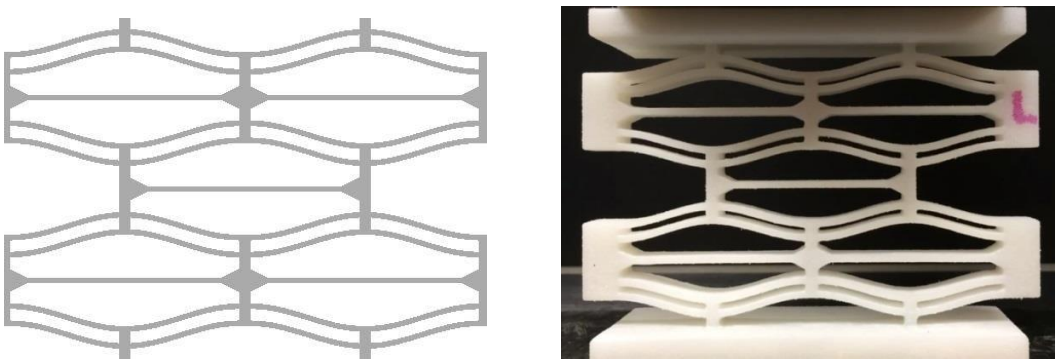

Figure 1.9: A representative honeycomb structure (Correa et al., 2015)

However, while these elements did exhibit the desired characteristics of an impact isolation structure, they perform best only when the load is applied perpendicular to the base. They are not suited for out of plane loading conditions and it is quite possible that the structures could twist and eventually break under those conditions.

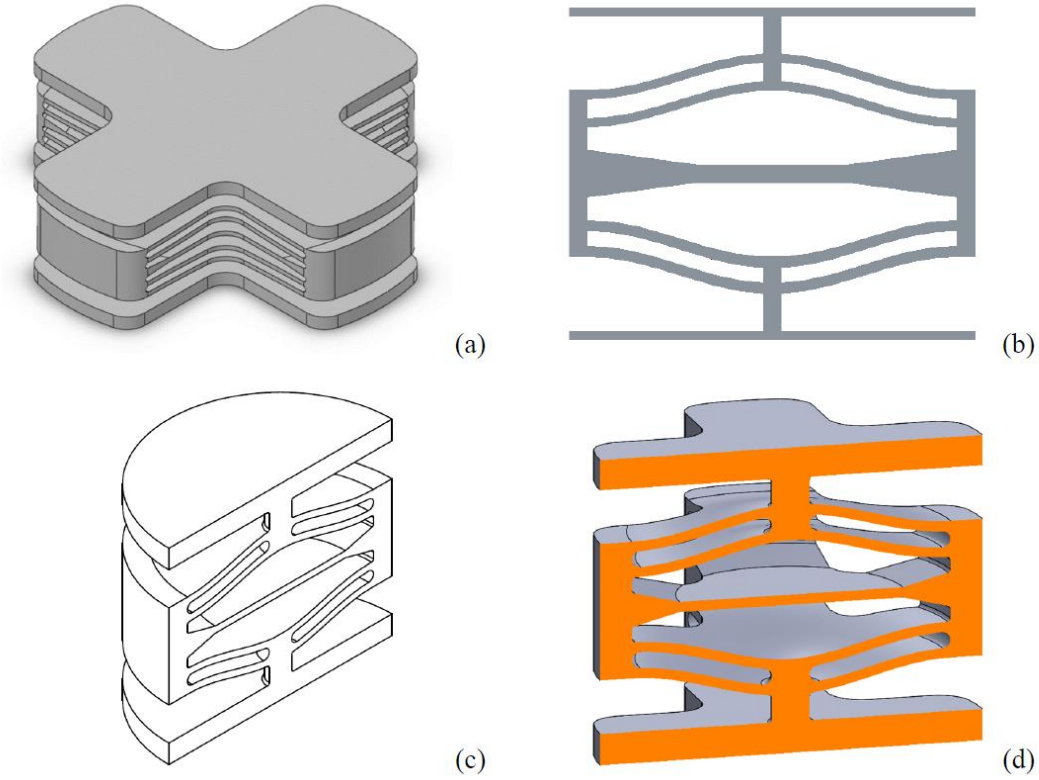

Figure 1.10: (a) Conformal Element, (b) 2D profile of the cross section, (c) Rotated profile around the central axis, (d) Mid – Section View.(Debeau and Seepersad, 2017)

In order to counter the above shortcomings, Debeau and Seepersad (2017) conceptualized a conformal design for the negative stiffness elements. The conformal designs were obtained by rotating the profile shown in Figure 1.10 (b) 360° about its central

axis (Figure 1.10 (c)) and cutting out four sections symmetrically to obtain the final design as shown in Figure 1.10 (a). This design also has the advantage that it can be used on a variety of curved surfaces and multiple elements can be arranged in a tiled pattern. Metal specimens of this design were manufactured and have been extensively investigated by Debeau and Seepersad (2017). This design has exhibited excellent impact mitigating properties even for repeated impacts. Due to the versatility of the design and its ability to recover from repeated impacts, the conformal design of negative stiffness element was a great starting point for this research.

1.3 Research Objectives

The primary goal of this research is to study the implementation of conformal negative stiffness honeycomb structures for impact isolation in baseball helmets. Original negative stiffness structures based on curved beams could bend out of plane and break when the line of impact is not orthogonal to the base. The conformal negative stiffness honeycombs help in overcoming this restriction. In this research, the aim is to optimize the design of these conformal elements and incorporate these modified conformal designs into a padding that can be used in baseball helmets and caps for providing better protection against impacts. The designs are investigated using finite element analysis and compared with experimental results. The manufactured elements are evaluated both quasi – statically as well as dynamically in a drop test rig and their performance are compared to conventional padding.

One of the other goals of this research is to investigate the design of the conformal structures to provide variable force thresholds to accommodate a larger range of impact

magnitudes and provide better protection. Another goal is to improve the existing understanding of these conformal designs by further investigation of their application.

1.4 Overview Of Thesis & Research

Significant research has been done on negative stiffness honeycomb structures. Chapter 1 covers some of the key instances found in literature. It is the first step in the direction of this research and helps in developing a sound understanding of the negative stiffness structures and the underlying principles. Chapter 2 covers the design aspect of the negative stiffness elements, the important design parameters, and the governing equations. The effect of these parameters on the design is also discussed. The implementation of conformal designs for impact isolation in headgear is also covered. The design of the conformal negative stiffness elements is analyzed using FEA in ABAQUS. The methodology and results are discussed in Chapter 3. Chapter 4 describes the physical testing of the conformal elements. The elements are tested both quasi-statically and dynamically and the results are compared with those from FEA. The performance of these elements are also compared against a conventional shock absorbing medium under the same loading conditions.

Chapter 2: Design of Conformal Negative Stiffness Elements

2.1 Introduction

This chapter focuses on the design aspect of the conformal negative stiffness elements (referred to as conformal elements throughout the rest of the thesis). In the previous chapter, important governing equations of a pre-curved beam were introduced. They are further discussed in the context of conformal designs. The initial design and the important design parameters that affect the performance characteristics of these conformal elements are also discussed. Research on the implementation of negative stiffness elements has primarily focused on using pre-curved beams having a constant force threshold. However, pertinent to this application a requirement of conformal elements having variable force threshold was identified. Hence, conformal elements with variable force threshold were designed. The method to introduce variable force threshold into negative stiffness structures is also discussed in this chapter.

2.2 Pre-Curved Beams: Important parameters and Relationships

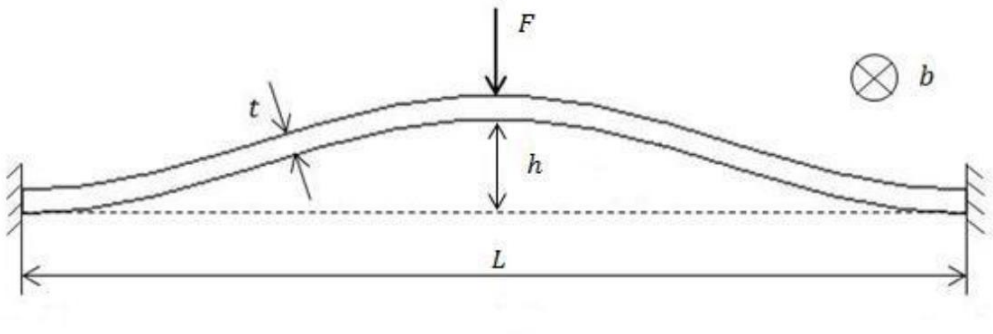

Figure 2.1: Pre-curved beam (Qiu et al., 2004)

As mentioned in Chapter 1, Qiu *et al.,* (2004) researched the use of pre-curved beams as a bi-stable mechanism and formulated a set of governing analytical equations.

The geometry of the proposed pre-curved beam as shown in Figure 2.1 is given by the following equation.

$$\overline{w} = \frac{h}{2}[1 - cos\left(2\pi\frac{x}{L}\right)] \qquad (2.1)$$

where, h is the maximum height of the beam, L is the length of the beam, x is the distance from the left end of the beam and $\overline{w}$ is the corresponding transverse height of the beam at a distance x. The normalized force displacement relationship is given by:

$$F = \frac{3\pi^4 Q^2}{2}\Delta\left(\Delta - \frac{3}{2} + \sqrt{\frac{1}{4} - \frac{4}{3Q^2}}\right)\left(\Delta - \frac{3}{2} - \sqrt{\frac{1}{4} - \frac{4}{3Q^2}}\right) \qquad (2.2)$$

where F and Δ are normalized force and normalized displacement respectively. Qiu *et al.,* (2004) also defined an important parameter called the Q ratio indicative of the behavior of the beam given by:

$$Q = \frac{h}{t} \qquad (2.3)$$

where t is the thickness of the beam. The normalized force F is related to the applied transverse force *f by* the following equation:

$$F = \frac{fL^3}{EIh} \qquad (2.4)$$

where E is the Young's modulus and I is the second moment of area of the cross-section. The maximum strain ε during deflection can be approximated as:

$$\varepsilon \approx 2\pi^2\frac{th}{L^2} + 4\pi^2\frac{t}{3L^2} \qquad (2.5)$$

All the above relations are also applicable for the conformal designs.

2.3 CONFORMAL NEGATIVE STIFFNESS ELEMENT DESIGN

The conformal negative stiffness design is obtained by revolving the standard curved beam negative stiffness profile and cutting the corners out so that it is easier to remove the powder when manufactured by powder bed fusion process and to tile the elements easily (Debeau and Seepersad, 2017). As a result, the conformal design closely resembles two standard curved beam negative stiffness structures overlapped at 90 degrees as shown in Figure 2.2.

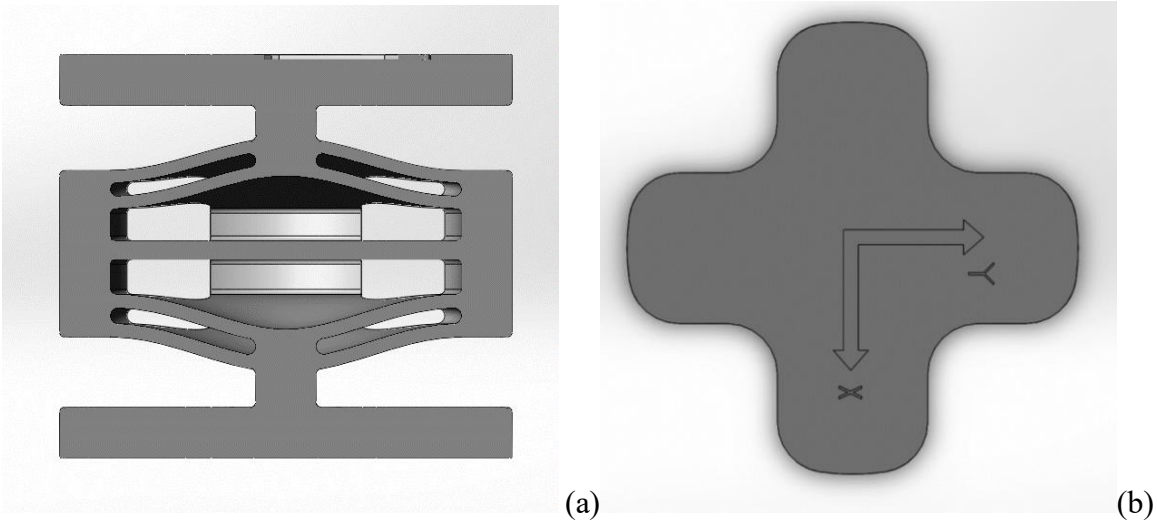

(a) (b)

Figure 2.2: CAD model representation of a conformal element (a) section view (b) top view.

The conformal designs utilize the pre-curved geometry proposed by Qiu *et al.,* (2004). The initial curved shape of the beam is according to the first mode shape of a buckled beam (Debeau and Seepersad, 2017). The properties and analytical equations presented in the previous sections are also applicable. For our application the elements

need to recover from the impact, hence mono- stability is a requirement. The theoretical Q value has to be less than 2.31 to achieve mono-stability. The important parameters that affect the performance of the beam are thickness ‘t’, length ‘L’, and height ‘h’ of the beam. If the thickness of the beam is increased the force threshold also increases. As described earlier, force threshold is the applied force after which the beams snap through. Increasing the length of the beam reduces the maximum strain developed in the beams as well as the force threshold (Debeau and Seepersad, 2017). The force threshold can be calculated by the Equations 2.2, 2.3 and 2.4. These equations estimate the force of one pre-curved beam. Since there are two concentric curved beams the force threshold of the element can be obtained by doubling the force threshold of a single beam (Debeau and Seepersad, 2017). The various sections of the conformal elements are as shown in figure 2.3.

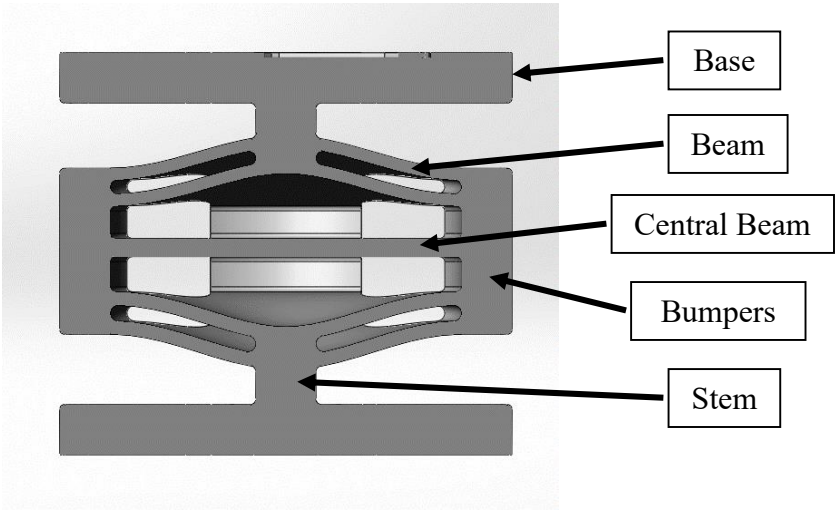

Figure 2.3: The sections of conformal element as labelled.

Certain design guidelines for the conformal elements have also been prescribed by Debeau and Seepersad (2017). The concentric beams are joined together at the center

to enable the beams to buckle from first mode to the opposite symmetrical mode via a third mode of buckling which assists in increased force threshold. The stem diameter should be adequate to prevent shear during quasi-static loading and should be adequately adjusted according to the application or any non-orthogonal impacts. Further, the bumpers should be of adequate thickness to prevent any bending when the beams buckle from one state to other.

2.4 Concept Design Of Conformal Element Specific To Application

2.4.1 Initial design and evaluation

The driving factor in designing a conformal element is the prescribed force threshold. The design must be optimized such that the beams neither exhibit a force threshold so low that they snap through for small impacts and cannot absorb moderate or higher impacts, nor exhibit a force threshold so high that they do not buckle for moderate impacts which may lead to serious injury. It is important to note that the enhanced impact absorption is because of the snap through behavior exhibited by the elements. However, one of the challenges in designing conformal elements for helmet applications is that the precise force threshold is unknown. Hence, instead of designing for the force threshold, the elements were modeled around an energy requirement of a one dimensional impact on the top of the head, and assumptions were made accordingly. In order to simulate an average one dimensional impact commonly observed in baseball or the construction industry, a 9.45 kg combined mass of head form, and testing hardware was dropped from a height of 12 inches and its potential energy was taken into account. The potential energy calculated was 27 Joules which is equivalent to a 145 g baseball travelling at a velocity of 19.3 m/s. This was to be absorbed by four conformal negative stiffness elements tiled together as

shown in figure 2.4. The elements were designed for this loading condition because this type of load could be applied with the existing testing equipment.

Figure 2.4: Four conformal NS elements tiled together.

Another constraint on the design was the overall height of the elements themselves. The height of the elements must be such that they could fit inside the helmet while still allowing room for the head form to fit comfortably. Taking into account the above assumptions and constraints, the conformal design was analyzed in ABAQUS. To build the model, a code developed by David. A. Debeau was implemented. A check was performed on the elements under the impact of a mass of 5 kg dropping on the elements with an impact velocity of 1.5 m/s and it was ensured that the elements did not bottom out during the impact. The material used was nylon 11. The final dimensions of this design are as given in Table 2.1.

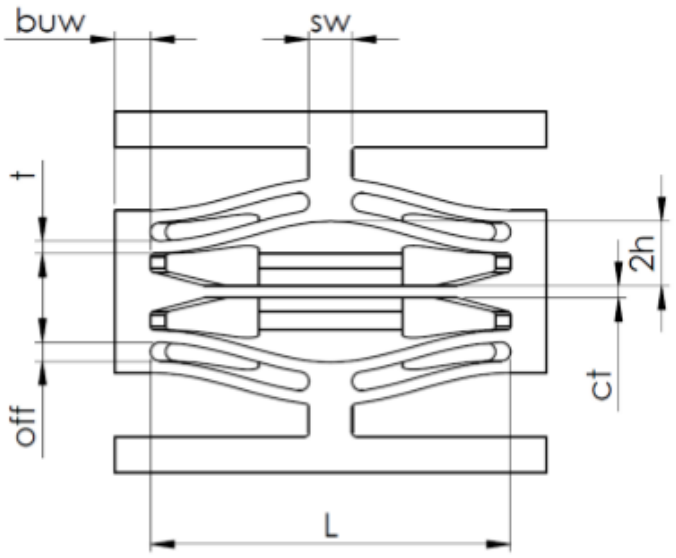

Figure 2.5: Cross section of the beam depicting the various measurements (Debeau & Seepersad, 2017).

Critical Dimension	Value (mm)
Beam Thickness (t)	1.45
Center Thickness (ct)	1.80
Beam Length (L)	35.0
Q Factor (Q)	2.41
Beam Height (h)	3.40
Beam Offset (off)	1.8
Bumper Width (buw)	5.00
Stem Width (sw)	6.00

Table 2.1: Critical dimension of conformal NS element.

The Q factor for the curved beams in this design was 2.41. Although, for the beams to be mono-stable the theoretical Q value should be less than 2.31, experiments have shown that for Nylon 11 mono-stability has been exhibited by pre-curved beams with Q values as high as 2.71 (Debeau and Seepersad, 2017). The overall height of the elements was 37.30 mm. It also includes the bases which are each 5 mm thick and can be re-purposed to include a lining of foam or silicone for comfortable fit and integration. A test was designed to evaluate and benchmark the performance of the conformal elements and also compare it to performance of conventional padding from a baseball helmet which meets NOCSAE standards. The elements were subjected to quasi–static testing and impact tests for performance evaluation, the results of which are discussed in Chapter 4. Impact tests conducted on individual conformal NS elements from various drop heights showed that the conventional padding in the sample baseball out-performed the conformal NS elements in impact mitigation for small impacts. For higher impacts the NS elements performed better than conventional padding. However, there was a need to make them more efficient.

2.4.2 Conformal element design with variable force thresholds

Based on the results of the impact tests done on the conformal NS elements, it was clear that the elements engaged for only a very small range of impact magnitude. Below that level of impact the negative stiffness elements did not engage or snap through, hence were unable to absorb the impact. So far, all the negative stiffness elements designed have been to accommodate only one certain peak threshold. Although the parameters could be adjusted to reduce the force threshold to make the beams snap through for impacts of smaller magnitude, it would lead to the elements getting fully compressed or bottoming out for even medium impacts.

Similarly, if the elements were designed for higher impacts they would be ineffective for medium or smaller impacts because the beams would not engage. To make these conformal elements to be effective for this application, there was a need to modify the design to accommodate a larger range of impact magnitudes. As discussed earlier, the force threshold determines when the beams snap through. To increase the range of impacts absorbed, the elements were required to have both a smaller force threshold value for smaller impacts and a larger force threshold value for impacts of larger magnitudes.

As discussed earlier, the force threshold is determined by the geometric parameters of the curved beams and there are various methods to control the force threshold of the beams. For our application the length of the beams were kept the same and the thickness and apex height of the beams were varied. Two designs were considered to include variable force thresholds in the conformal elements.

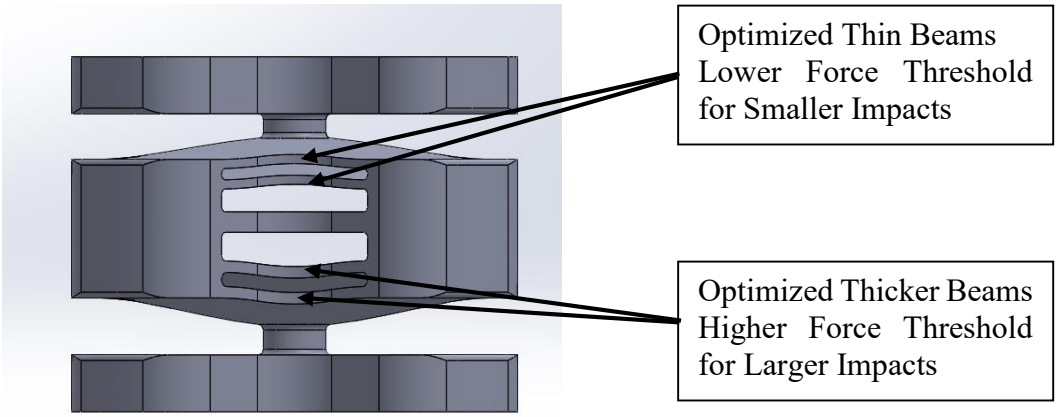

(a)

Figure 2.6: Concept design of conformal elements with variable force threshold –
(a) Standard structure.

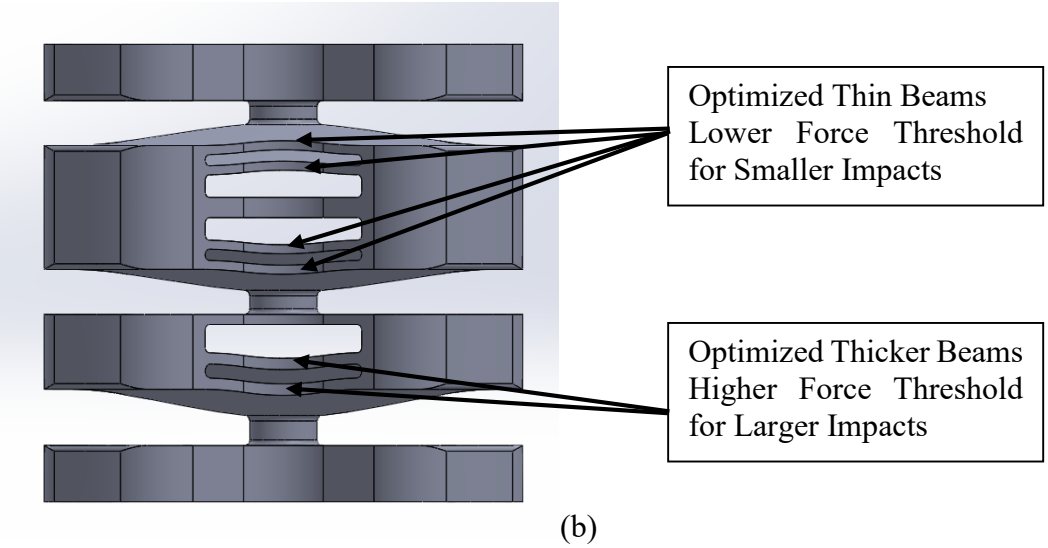

Figure 2.6 (contd.): Concept design of conformal elements with variable force threshold – (b) Multi-layered structure.

Figure 2.6 shows the two designs with variable force thresholds. In the concept design as shown in figure 2.6(a), the upper concentric beams are thinner and their apex height has been adjusted according to the desired Q ratio while the lower concentric beams are thicker and their apex height has also been adjusted according to the desired Q ratio. As a result, the conformal elements have two force thresholds to accommodate the smaller and larger impacts. Experiments with negative stiffness structures have shown that increasing the number of layers of pre curved beams helps in better impact absorption (Debeau *et al.,* 2018). The layered design concept shown in Figure 2.6 (b) offers that advantage. In this design a standard conformal element is layered over another element. The beam thickness and height of each layer can vary according to the application. The Q ratio must be taken into consideration to prevent any bi-stable behavior. Some samples of these conformal element designs were also manufactured by SLS as a proof of concept as shown in Figure 2.7. Manual compression clearly exhibited the force threshold variability.

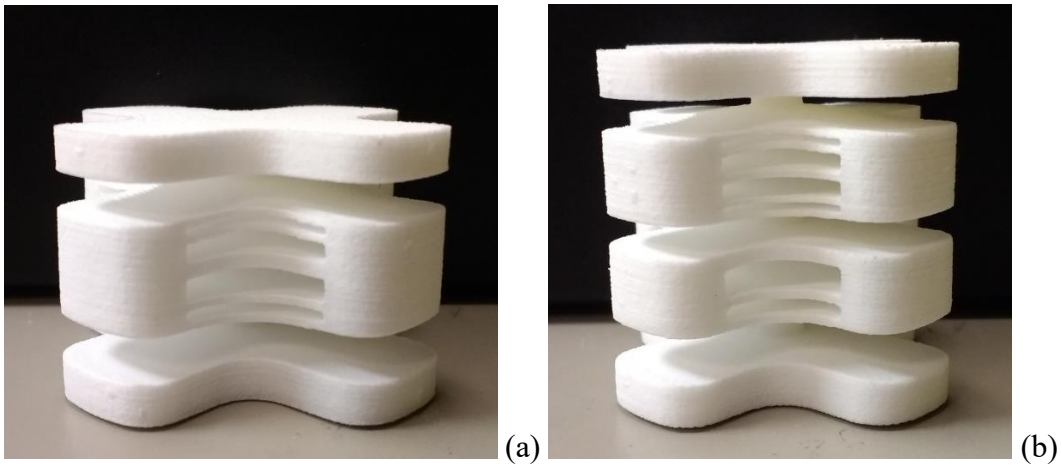

Figure 2.7: Manufactured prototypes - (a) Standard conformal structure (b) Multi-layered structure.

Due to the constraint on the height, the layered structure (as shown in figure 2.7 (b)) was not selected for our application. For optimization, simulations were carried out in ABAQUS for lower impact magnitude with a 5 kg mass falling at a velocity of 1.1 m/s, which is similar to the weight being dropped from a height of 3 inches approximately, as a check to ensure that the beams snapped through for smaller impacts. The resulting force threshold was obtained using quasi-static analysis in ABAQUS. The thickness of the thicker beam was increased so that the total energy absorption of the element under quasi-static analysis was not reduced as compared to the initial conformal elements.

2.5 Material Selection

The modified conformal elements were manufactured with selective laser sintering (SLS) in nylon 11 material. For our application, the elements were manufactured using polymers rather than metals because of the force threshold requirements. The most commonly used polymers with a powder bed fusion process such as SLS are nylon 11 and nylon 12. Nylon 11 has high impact resistance, good elasticity and high elongation at break.

Nylon 12 has a higher Young's modulus as compared to nylon 11; so, if the elements were manufactured out of nylon 12, the beams must be thinner, requiring a higher resolution manufacturing capability. Hence, nylon 11 was used. During the design of these elements it is also important to check the parameters such that the strain in the beams during deflection does not exceed the yield strain of the material. The yield strain during deflection is estimated by the following equation (Qiu *et al.*, 2004). The yield strain value obtained from previous builds was approximately 0.10, which was set as the yield strain limit for this application. The strains obtained for the beams are tabulated in Table 2.2.

$$\varepsilon \approx 2\pi^2 \frac{th}{L^2} \quad (2.6)$$

	Thickness (t) mm	Height (h) mm	Length (L) mm	Strain
Beam 1	1.35	3.25	35.00	0.0707
Beam 2	1.50	3.50	35.00	0.0846

Table 2.2: Strain values for designed conformal elements.

The final design dimensions of the conformal elements are documented in Table 2.3.

Critical Dimension	Value (mm)
Beam Thickness thin	1.35
Beam Thickness thick	1.50
Center Thickness	1.80
Beam Length	35.0
Q factor	2.40
Thin Beam Height	3.25
Thick Beam Height	3.50
Beam Offset	1.6
Bumper Width	5.00
Stem Width	6.00

Table 2.3: Critical dimension of conformal NS element with variable force threshold.

2.6 Manufacturing Of The Elements

Four elements were manufactured by Selective Laser Sintering with the help of Stratasys Direct Manufacturing. The material used was nylon 11 with a layer thickness of 0.004 inches. The elements were manufactured in the upright position with the XY plane as marked on the elements (figure 2.8) aligned with the XY plane of the build platform.

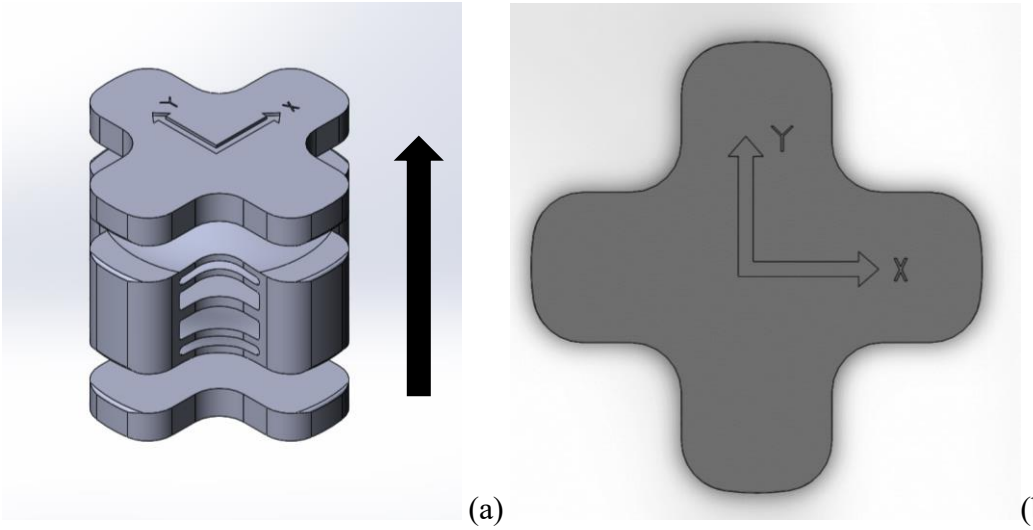

(a) (b)

Figure 2.8: Orientation of the part during manufacturing (a) Upright Position (b) XY marked on the part oriented with the build platform.

Two tensile bars (following the ASTM D638 standard) were also manufactured alongside these elements to obtain the mechanical properties of the built product.

2.7 Integration Of The Elements Into Helmet Application

Using these conformal elements a padding can be developed as shown in figure 2.9. In baseball helmets strips of high density foam are used which are adhered to the inside wall of the helmets. Similar strips could be developed which integrate the conformal elements into the padding.

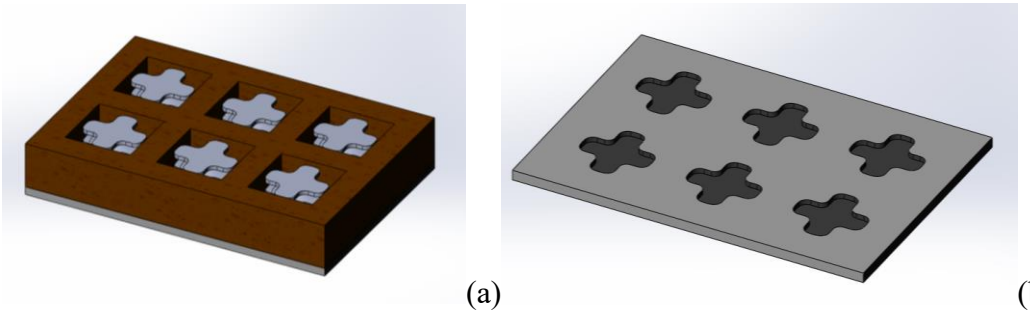

(a) (b)

Figure 2.9: Trimetric view of (a) a sample padding with integrated conformal elements. (b) Silicone rubber base

The padding shown in figure 2.9(a) consists of a 6 mm silicone rubber or a similar material lining as a base. Silicone rubber is relatively inert and resistant to extreme environments. Due to this property it is extensively used in apparels or in application involving skin contact. It is also easy to manufacture and shape. The base has 3 mm deep depressions matching the footprint of the conformal elements with suitable tolerances as shown in figure 2.9(b). The conformal elements are set in place on the rubber base with a suitable adhesive.

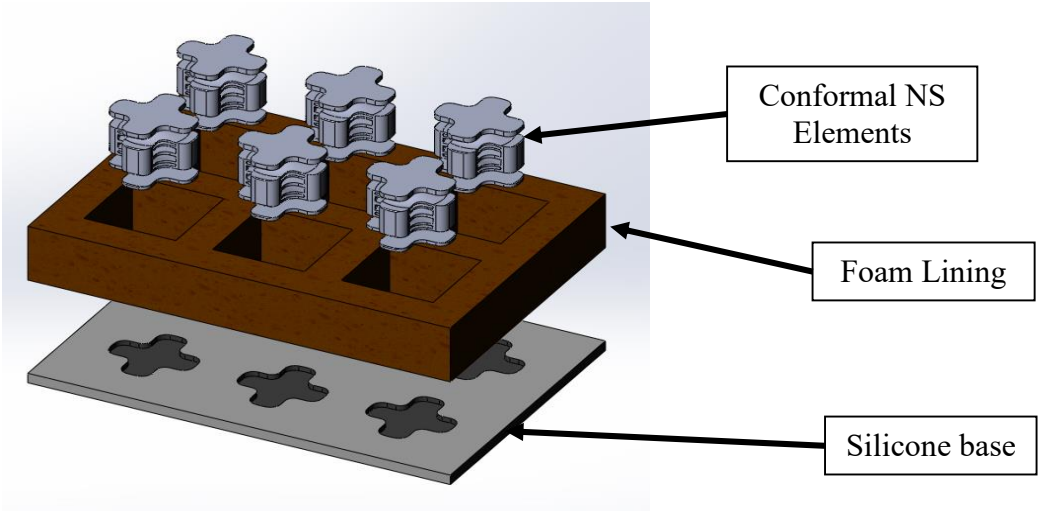

Figure 2.10: Exploded View of the padding.

The spacing between the elements should be sufficient to prevent any contact between two adjacent elements as it will impair their ability to compress. The spaces between the elements are filled using a foam similar to that used in conventional padding. The foam is adhered to the silicone rubber base.

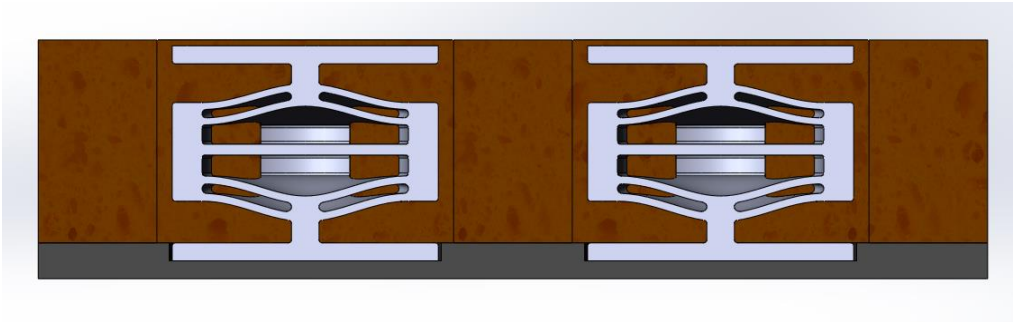

Figure 2.11: A section view of the padding.

The padding is then adhered to the inside of the helmet wall through the foam. The thickness of the base of the conformal elements was reduced from 5 mm to 2 mm. As can be seen in figure 2.11 the conformal elements are set about 1 mm lower than the surface of the foam. This is to ensure that one of the ends of the conformal NS elements is free and is not adhered to the helmet wall, to prevent application of significant lateral forces on the bases of the conformal elements. The overall height of the padding is 38 mm which is a bit on the higher side as compared to height of conventional padding which is 27 mm approx..

2.8 SUMMARY

In this chapter the various analytical equations governing the pre-curved beams are covered in detail, along with the basic arrangement of the conformal design. The initial design of a conformal element is also explained followed by the need to have elements with variable force threshold. The method to introduce variable force threshold is also

developed along with two concept designs that can be implemented. The manufacturing and material selection of the conformal elements are also discussed, followed by a concept design to integrate the conformal elements into a padding.

Chapter 3: Finite Element Analysis

3.1 Introduction

In the previous chapter a conformal element with variable threshold was designed and developed. In this chapter the design is further analyzed using finite element analysis (FEA) in ABAQUS. The critical dimensions of the manufactured element are measured and documented. The material properties are obtained, and assembly and boundary conditions are defined. The conformal elements are subjected to both quasi-static as well as impact loading conditions. Finally, the results of the analyses are presented.

3.2 Modeling Of The Conformal Element

As described earlier the elements were manufactured using SLS. Figure 3.1 shows the manufactured parts. A tensile bar was also manufactured alongside the elements to ascertain the mechanical properties of the built parts.

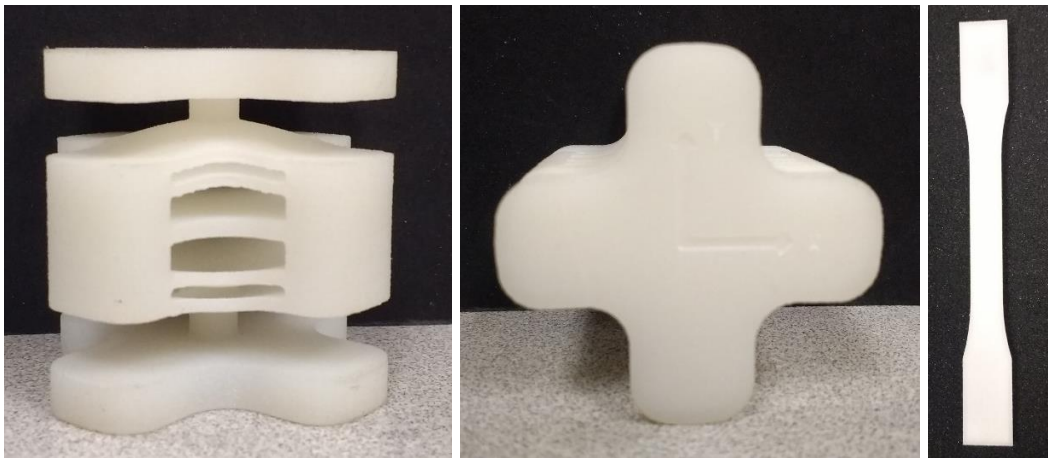

Figure 3.1: Manufactured conformal elements and tensile bar specimen.

The dimensions of the built parts are tabulated below. The dimension labels are as described earlier in Figure 2.5.

Critical Dimension	**Value (mm)**
Beam Thickness thin	1.40 ± 0.1
Beam Thickness thick	1.54 ± 0.1
Center Thickness	1.80
Beam Length	35.0
Q factor	2.3 (approx)
Thin Beam Height	3.25
Thick Beam Height	3.50
Beam Offset	1.60
Bumper Width	5.00
Stem Width	6.00

Table 3.1: Dimensions of the manufactured conformal elements.

Using the dimensions given in Table 3.1, an initial model of the conformal element was generated in ABAQUS with the help of a code devised by David Debeau. This model was further developed to incorporate the variable height and beam thicknesses. The developed model is easily modifiable to incorporate different beam thicknesses. The modeled conformal element is shown in Figure 3.2.

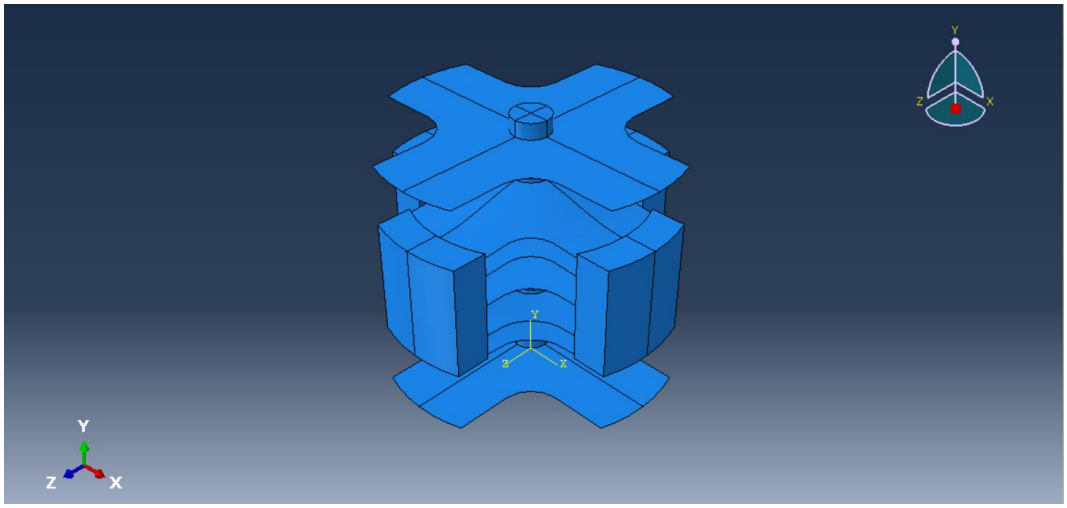

Figure 3.2: Modeled conformal element with solid and shell elements.

3.2. Material Selection And Properties Of Conformal Elements

As discussed in Chapter 2, nylon 11 was used to manufacture the conformal elements. A tensile bar specimen was manufactured and subjected to tensile testing, and the stress – strain curve was obtained as shown in Figure 3.3. The tensile bar was oriented in the ZXY orientation (Brent Stucker, Univ. of Louisville, ASTM F42).

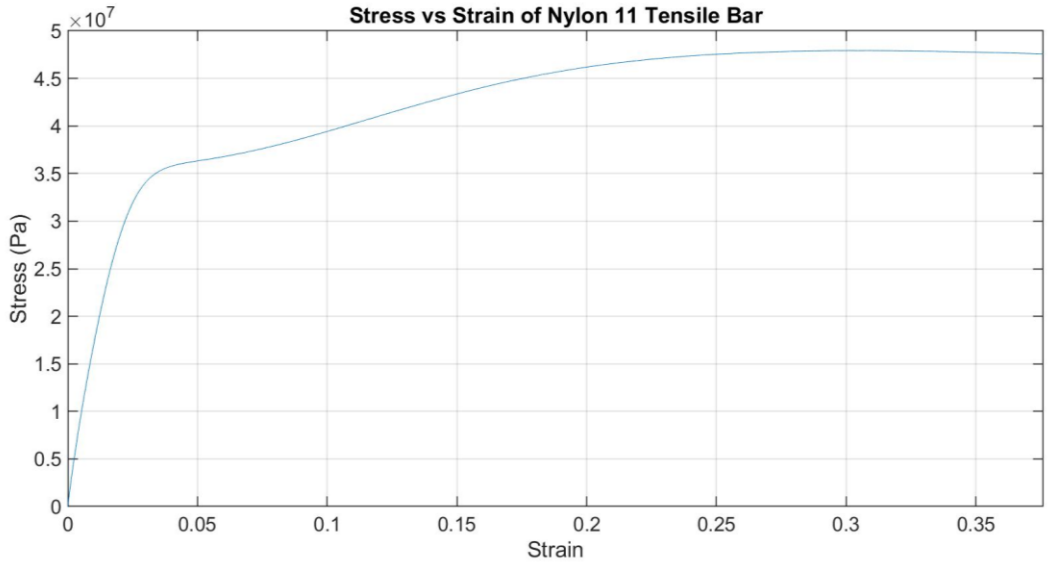

Figure 3.3: Stress strain curve of a tensile bar specimen built alongside the conformal elements.

The tensile testing was conducted on an Instron machine. Strain was measured with the help of an extensometer. It is an industry standard to conduct tensile tests of tensile bar specimens manufactured alongside the parts manufactured by SLS because the properties of additively manufactured parts are different from those of cast or injection molded parts and vary significantly from build to build. Based on the values obtained from the tensile test, the Young's modulus was found to be 1.55 GPa. The yield strength was found to be 31 MPa approximately.

For the purpose of analysis in ABAQUS, in addition to Young's modulus and Poisson's ratio, the true stress and true strain data are also required for analysis of any plastic deformation in the element. True stress and true strain can be calculated from nominal stress and nominal strain through Equations 3.1 and 3.2 respectively.

$$True\ Stress = Nominal\ Stress(1 + Nominal\ Strain) \qquad (3.1)$$

$$True\ Strain = \ln(1 + Nominal\ Strain) \qquad (3.2)$$

True stress as a function of true strain curve is shown in Figure 3.4. The curve was input into ABAQUS for analysis of any plastic deformation.

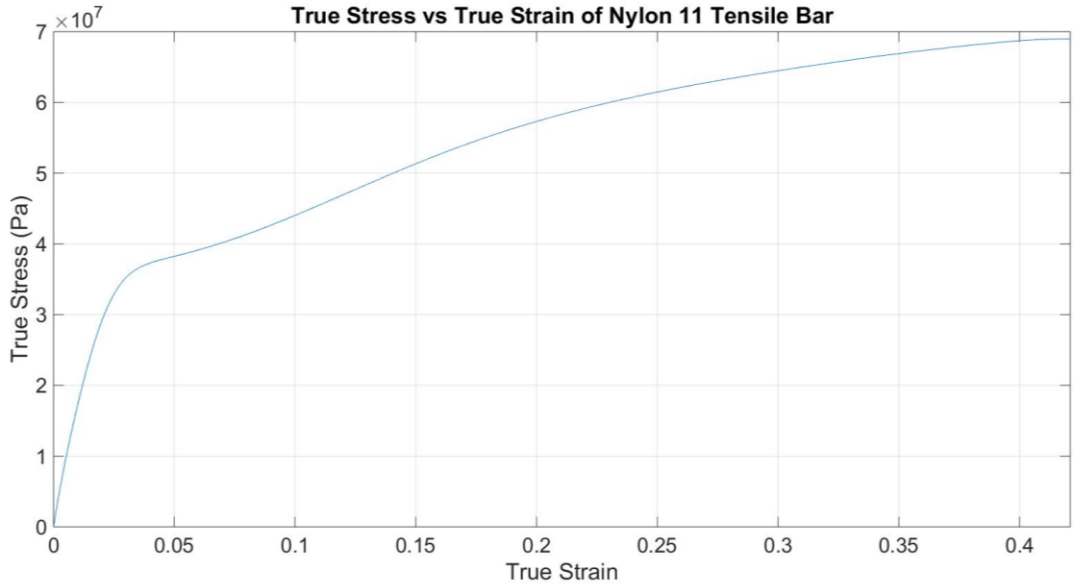

Figure 3.4: True Stress versus True Strain curve of a tensile bar specimen built alongside the conformal element.

3.3 Quasi-Static Analysis of the Conformal Elements

This section describes the quasi-static FEA analysis of the conformal elements in ABAQUS. In this section the assembly, interaction, boundary conditions and other aspects of the analysis are discussed.

3.3.1 Element types and meshing

Two kinds of elements were used for modelling the conformal elements. The beams and bases were modeled using shell elements. Shell elements were used because the thicknesses of the beams and base are significantly smaller than their other dimensions and because shell elements are advantageous in terms of computational cost and time. The rest of the conformal elements, such as the bumpers and the stem, were modeled using solid elements.

For meshing, a global element size of 0.5 mm was used. The analysis was initially started with an element size of 0.8 mm. The element size was refined to provide reasonable modeling accuracy without being too computationally expensive. As can be seen from Figure 3.5, the results started to converge around element size of 0.5 mm. For element size of 0.4 mm, the total CPU time for analysis was 28.33 hours while for element size of 0.5 mm it was 12.08 hours.

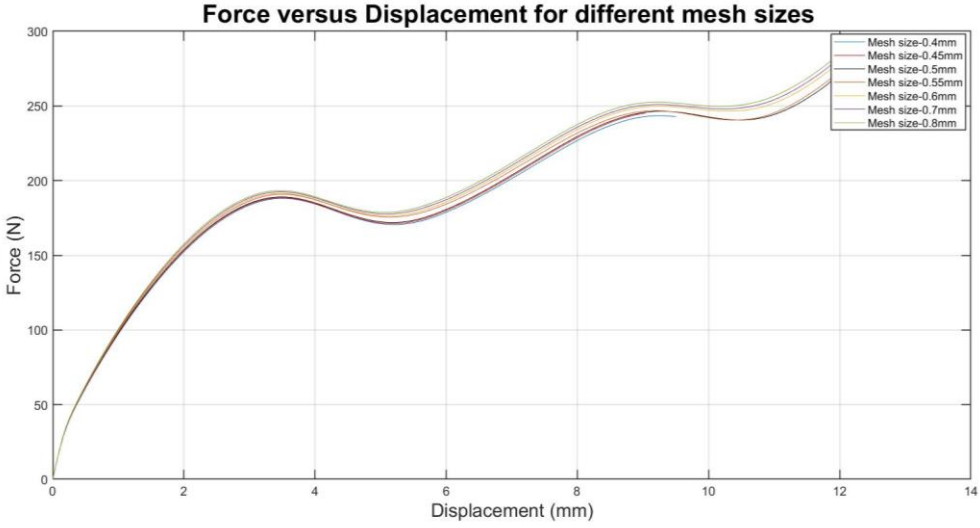

(a)

Figure 3.5: (a) Quasi static analysis results with element sizes of 0.8 mm, 0.7 mm, 0.6 mm, 0.55 mm, 0.5 mm, 0.45 mm, and 0.4 mm.

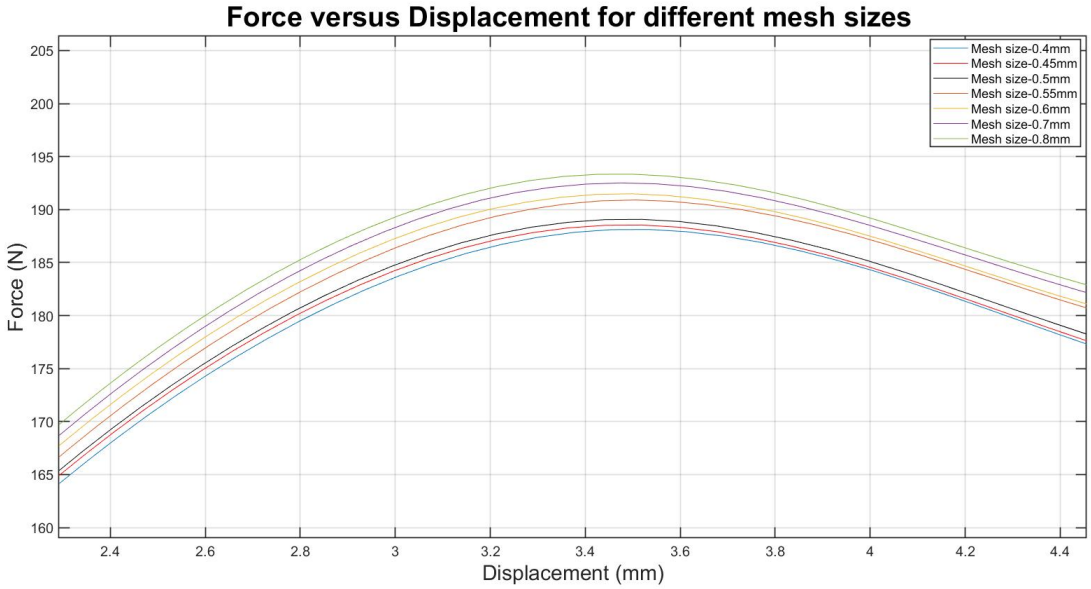

(b)

Figure 3.5 (contd.): (b) Magnified view of the Force versus displacement curve around first force threshold. The results converge for element sizes 0.5 mm, 0.45 mm, and 0.4 mm,

For solid portions, 8 node linear hexagonal brick C38DR meshing elements with reduced integration were used. In anticipation of excessive distortion of elements, enhanced hourglass control was used. The shell elements were meshed using S4R elements, a 4 node doubly curved shell, linear quadrilateral meshing elements with reduced integration and hourglass control. Figure 3.6 shows the meshed element.

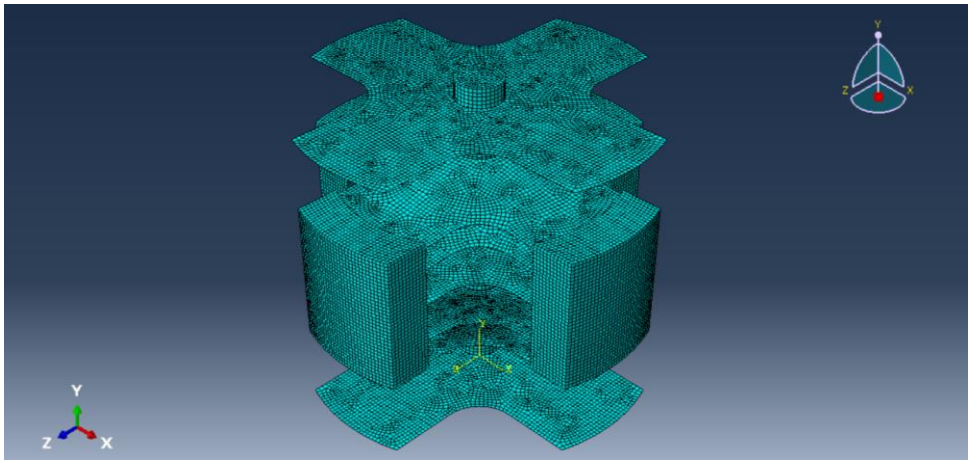

Figure 3.6: Meshed conformal element using solid and shell elements.

3.3.2 Constraints and interactions.

Since the model includes solid and shell elements, it is very important to define the interaction of the shell edge to the corresponding solid surface/ face so that their motion is coupled as shown in Figure 3.7. This coupling can be defined using the Shell to Solid Coupling type constraint from the Constraint option. For other sub options the default values were used.

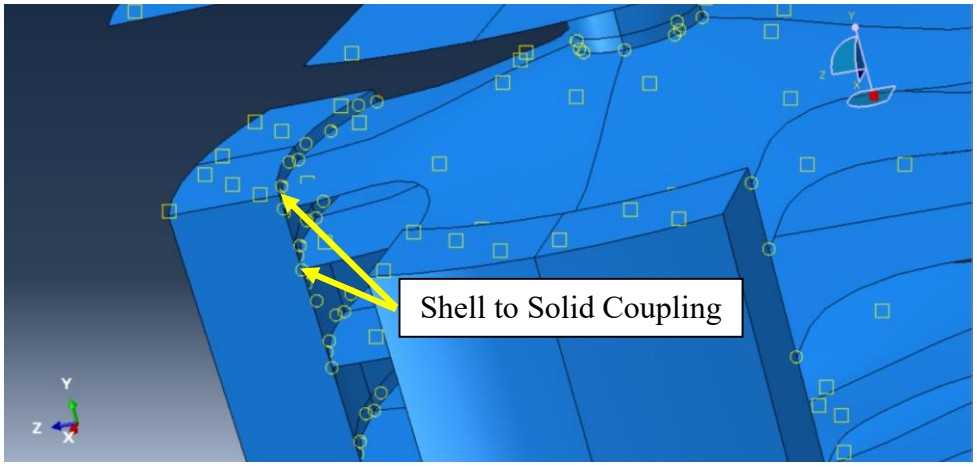

Figure 3.7: Defining shell to solid coupling.

In addition to specifying shell to solid coupling, the interactions between the different surfaces were also defined. The larger surface was defined as the master surface. The interaction property between these surfaces was defined as frictionless because of the negligible impact on the load versus displacement output as well as the very limited contact and motion between the surfaces.

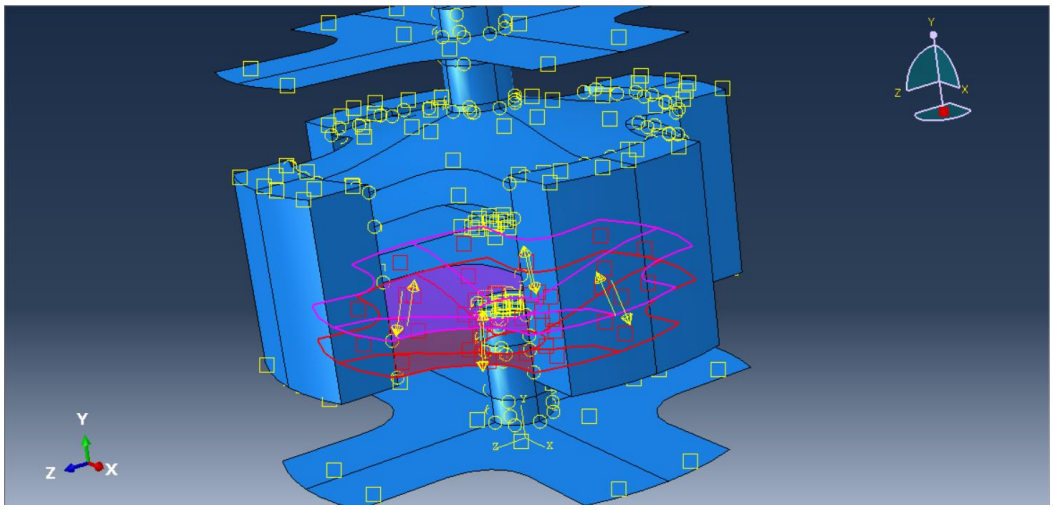

Figure 3.8: Defining surface interactions.

3.3.3 Loading and boundary conditions.

Two types of loads were defined on the conformal element. The initial reference load of 1000N was defined on the top surface of the element as shown in Figure 3.9, and a gravity field was specified.

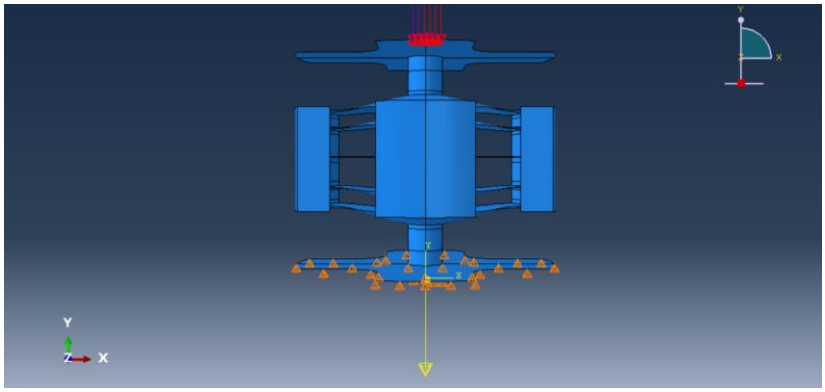

Figure 3.9: Loading and boundary conditions.

Pinned boundary conditions were defined in the X, Y, and Z axes on the bottom surface and edges in order to restrict the rotation of the element. This boundary condition allowed the element to deflect only in the Y axis, which would be the case in a physical quasi static analysis.

3.3.4 Assembly and analysis step.

One instance of the conformal element was used for quasi static analysis. During the analysis, large displacements and geometric distortions were expected due to the buckling or snapping-through of the pre-curved beams, hence non – linear geometry was used for analysis. The non-linear geometry option can be turned on or off through an option - Nlgeom in ABAQUS while defining the analysis step. For non-linear static analysis of buckling behavior, an algorithm called the modified Riks method available in ABAQUS was used. In this method ABAQUS solves iteratively for both load and displacement and uses another quantity called the arc length to measure the progress of the analysis. An initial reference load is defined which varies during the steps of the analysis by a factor called the load proportionality factor. The output is in terms of the load proportionality factor and the actual load can be calculated by Equation 3.3.

$$F_c = \alpha F_d \qquad (3.3)$$

where, F_c is the current load value, α is the load proportionality factor, and F_d is the initial reference load which is varied. The reference load in our case was assigned at 1000N. The displacement was also specified in this step. The maximum displacement of the element in the Y direction was set at 12 mm. The output database was defined to report the load proportionality factors for the entire analysis and the spatial displacement in the Y direction of a point on the top surface of conformal element.

3.3.5 FEA result of quasi-static loading

After defining the geometry, interactions, constraints, boundary conditions and mesh, the model was subjected to quasi-static analysis through the modified Riks method discussed earlier.

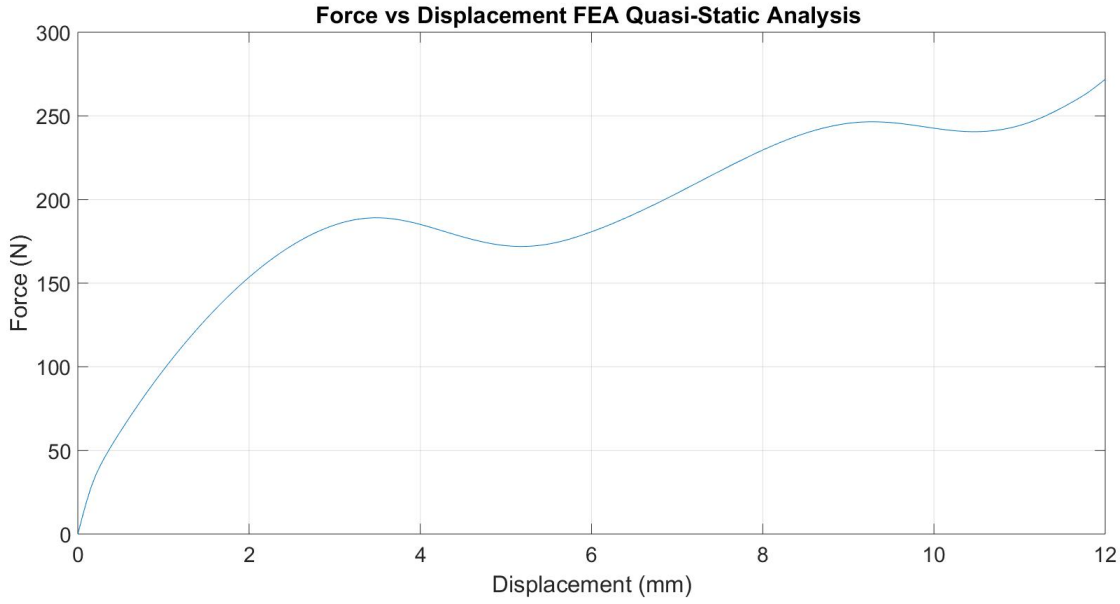

Figure 3.10: Force versus displacement graph obtained from quasi-static analysis through FEA in ABAQUS.

Figure 3.10 shows the force displacement curve obtained from the analysis. As was discussed during the design phase, these elements were expected to have two force thresholds. True to that prediction, two very distinct force thresholds were obtained after which each set of concentric beams snapped through to the opposing buckled position.

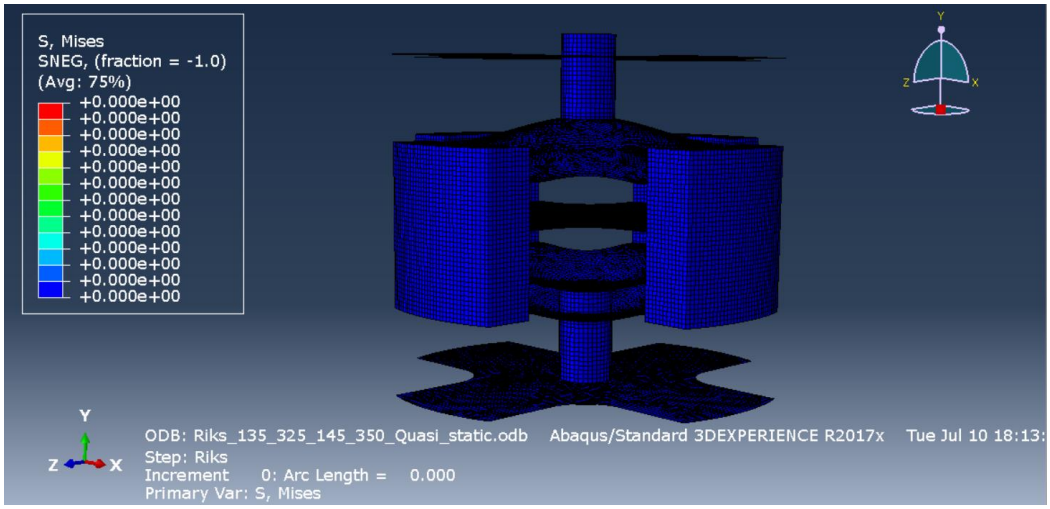

Figure 3.11: Stage-1: Element before the start of quasi-static analysis.

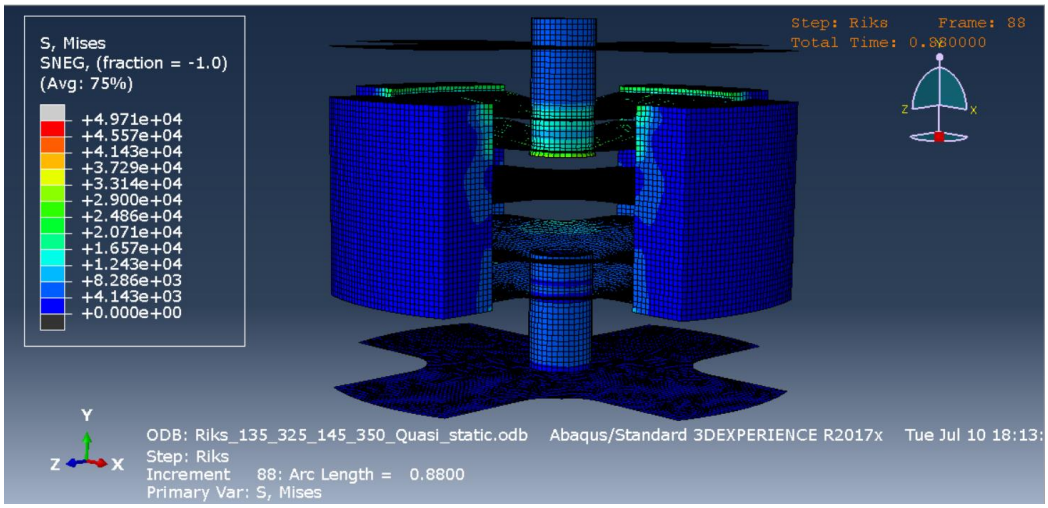

Figure 3.12: Stage-2: Thinner concentric beams snap through.

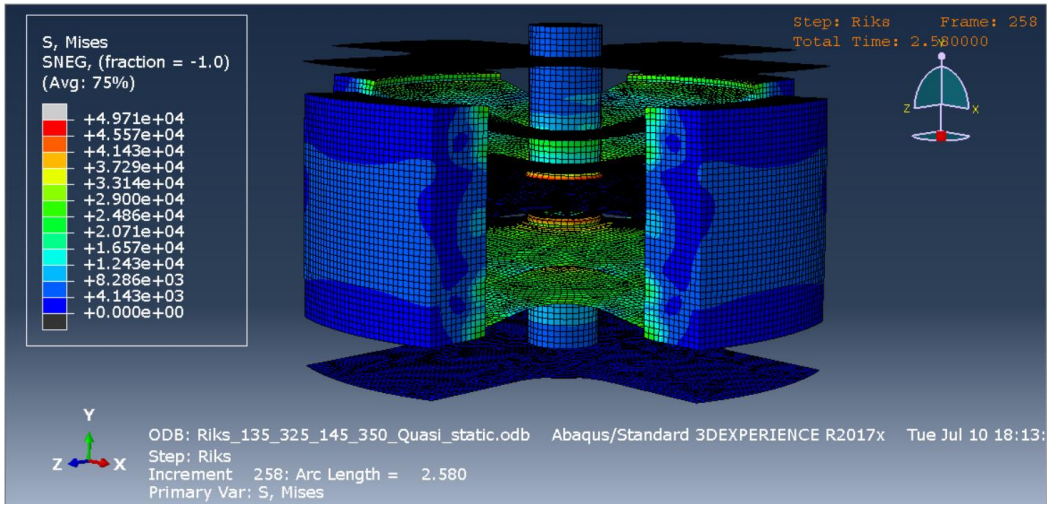

Figure 3.13: Stage-3: Element in fully compressed state. Both set of concentric beams snapped through.

FEA prediction for the Stage-1 buckling (as shown in Figure 3.12) was found to be 189.08 N while that for Stage-2 buckling (as shown in Figure 3.13) was 246.47 N. During maximum compression the maximum von Mises stress value obtained was 49.71 MPa which is well beyond the yield strength of the material. For further investigation, the contour shown in the output FEA model was modified to represent stress higher than the yield strength of 31 MPa in red to identify regions of high stress as shown in Figure 3.14.

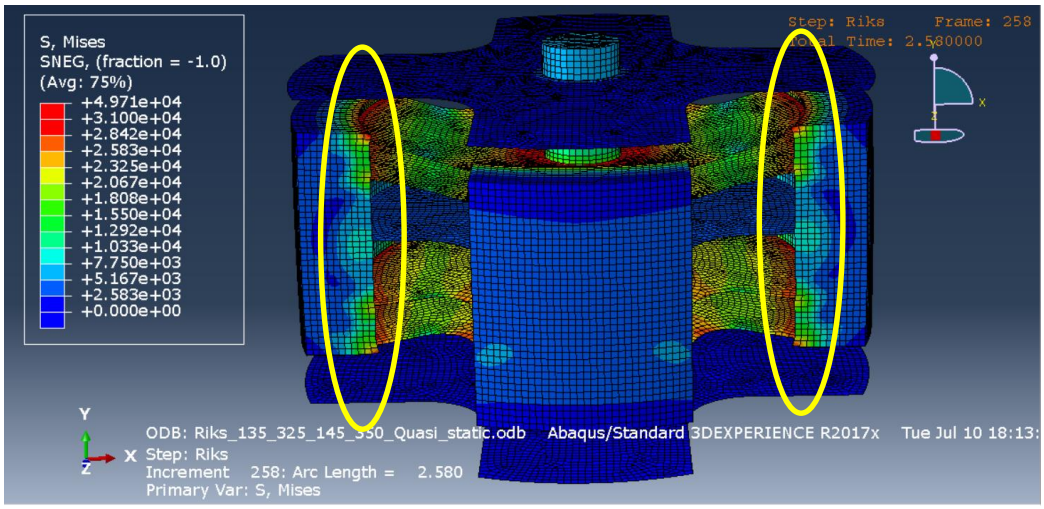

Figure 3.14: Stress contour of the conformal element. The encircled regions show regions of high stress

The high stress values were obtained at the sharp corners where shell to solid couplings have been defined. The sharp corners led to stress concentration in those areas. Fillets or chamfers were not provided in the model because the beams and bases were modeled as shells for computational efficiency, and they make it difficult to model fillets or chamfers. In physical samples, appropriate fillets and chamfers have been provided to relieve stress from these areas.

3.4 FEA Analysis of Conformal Elements Under Impact Loading

After the quasi-static testing, the elements were subjected to FEA analysis under impact loading conditions. Some of the material properties and analysis inputs were identical to those in the quasi-static analysis. Additional modelling and input parameters are discussed in this section.

3.4.1 Modelling the head form and the helmet.

For the purpose of impact testing, the existing testing set up comprised four conformal elements inside of a baseball helmet and positioned between the helmet and a head form. The mass of the entire assembly was 8.5 kg (hardware + head form), and it was dropped from various heights. The helmet shell and head form were modeled first.

The head form was modeled along the lines of a Humanetics Hybrid – III male head form. The dimensions were taken from an outline provided by the manufacturers shown in Figure 3.15. The head form was 204 mm in length, 183.20 mm at the widest part and the maximum height was 91.60 mm. The sketch of the cross-section along with the detailed dimensions is shown in Figure 3.16(a). The top half of the head form was modeled as a solid element as shown in Figure 3.16(b).

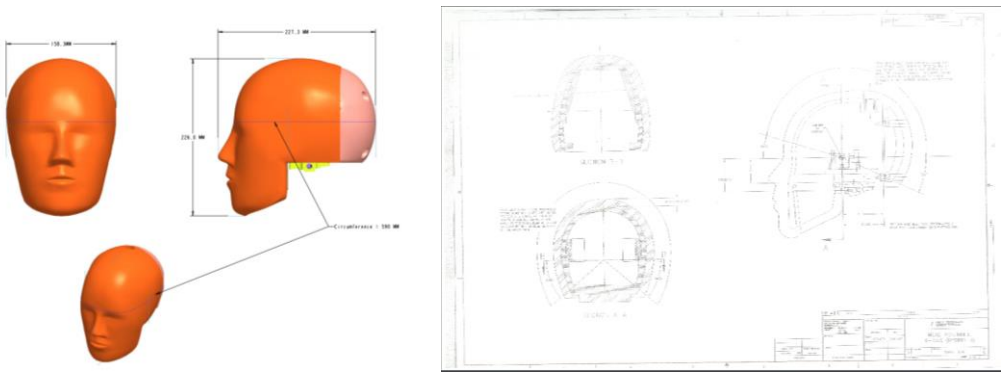

Figure 3.15: Humanetics Hybrid III male head form dimensions provided by manufacturers.

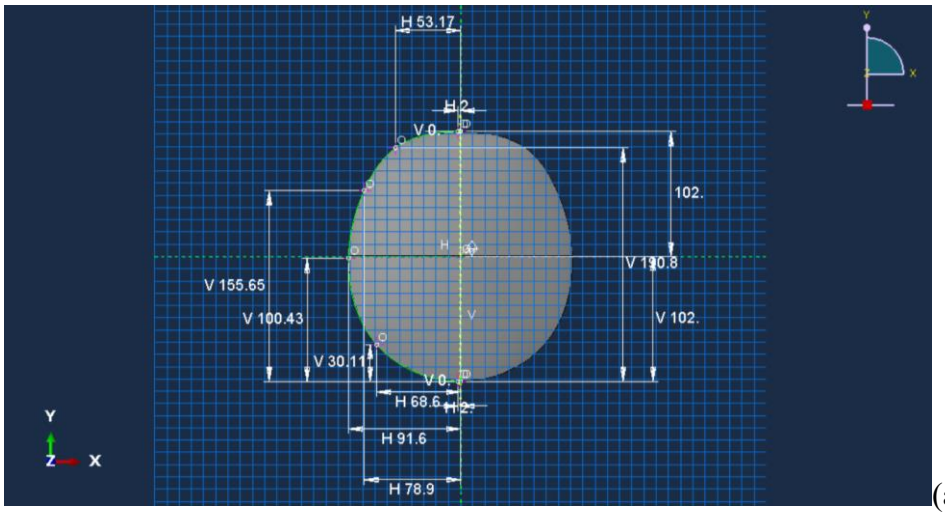

(a)

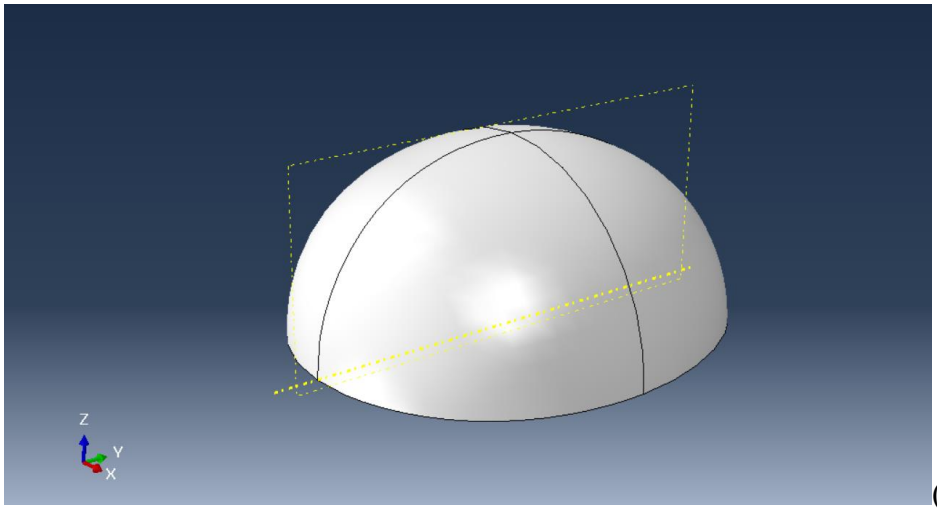

(b)

Figure 3.16: (a) Sketch of the cross-section of the head form. (b) Modeled top half of the head form.

Next, the helmet was modeled. Unfortunately, the exact dimensions of the helmet could not be procured; hence, measurements were taken manually so that the helmet geometry would be as accurate to the actual physical helmet as possible. The modeled helmet shell was 228.60 mm in length, 190.60 mm at the widest part and the maximum height was 114.30 mm. The sketch of the cross-section along with the detailed dimensions

has been shown in Figure 3.17(a). The thickness of the helmet shell was found to be 4.5 mm. Since the thickness was small compared to the other dimensions of the helmet, it was modeled as a shell element as shown in Figure 3.17(b).

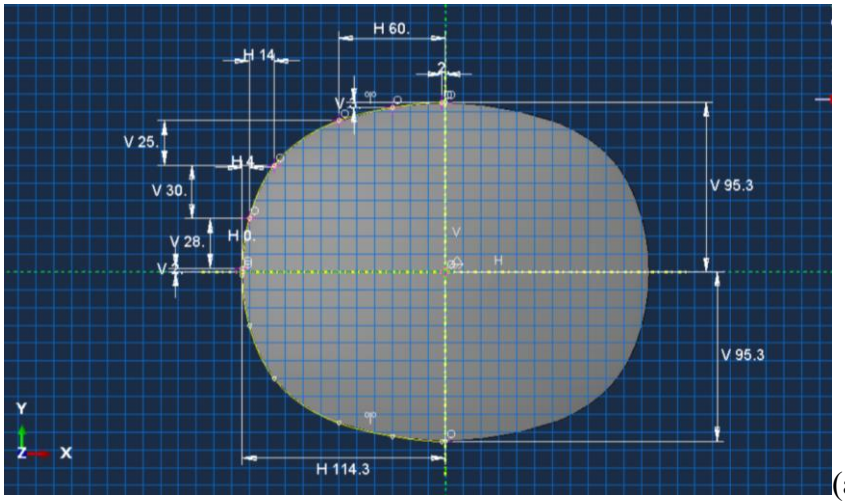

(a)

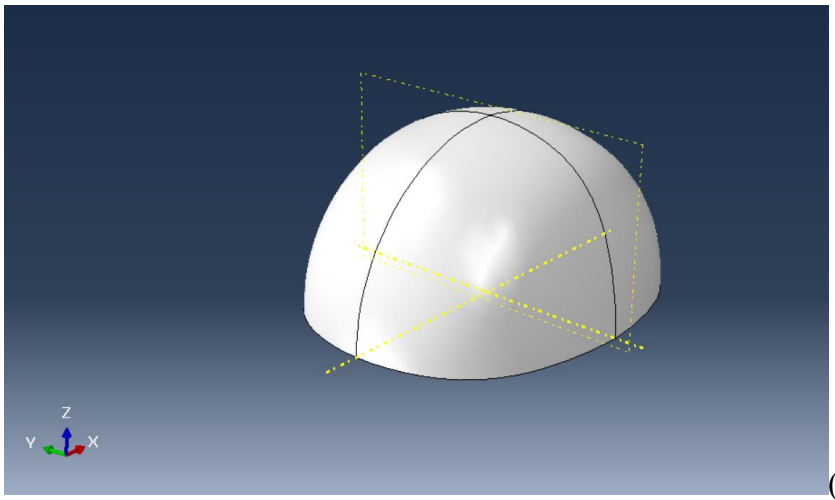

(b)

Figure 3.17: (a) Sketch of the cross-section of the helmet. (b) Modeled helmet

The conformal elements were modeled as discussed in the quasi-static testing section.

3.4.2 Material properties

The head form was additively manufactured in a Craftbot XL FDM machine using ABS material at The University of Texas at Austin. The infill percentage was 25% using a rectilinear pattern. The layer thickness was 0.20 mm with 4 shells. A tensile bar specimen was also manufactured from the same FDM machine using 100% infill and the same process parameters. The stress strain curve obtained from the tensile bar is shown in Figure 3.18.

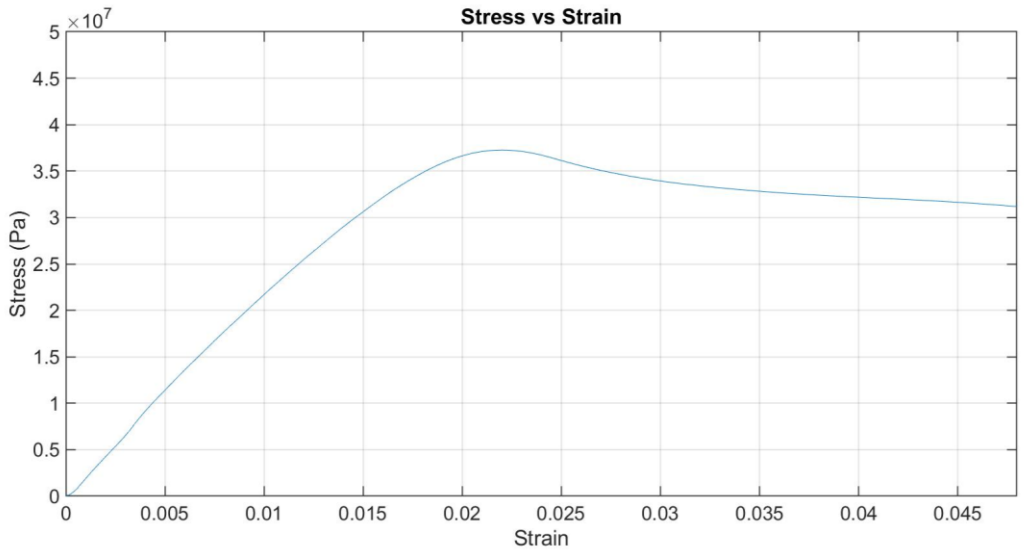

Figure 3.18: Stress- Strain curve of ABS tensile bar manufactured by FDM.

From the above stress strain curve the Young's modulus was calculated to be 2.3 GPa. However, the Young's modulus calculated is for 100% infill. Young's modulus for 25% infill was found with the help of a study conducted by Fernandez *et al.*(2016) in which tests were carried out to understand the effect of infill pattern and infill percentage on the

strength and stiffness of the tensile bar specimen. Using the data from the study, the Young's modulus for 25% infill was extrapolated to be 1.24 GPa.

For ascertaining the material properties of the helmet, a strip was cut from a representative helmet, and a tensile test was conducted on the sample. The strip was 110 mm long, 8.1 mm in width, and 4.4 mm thick. The stress-strain curve obtained from the tensile test is as shown in Figure 3.19. The calculated Young's modulus was 2.4 GPa, The material used for manufacturing the helmet was ABS as described in the product catalog of Rawling and the obtained Young's modulus was also within the range of 2 GPa to 4 GPa that is generally observed for ABS.

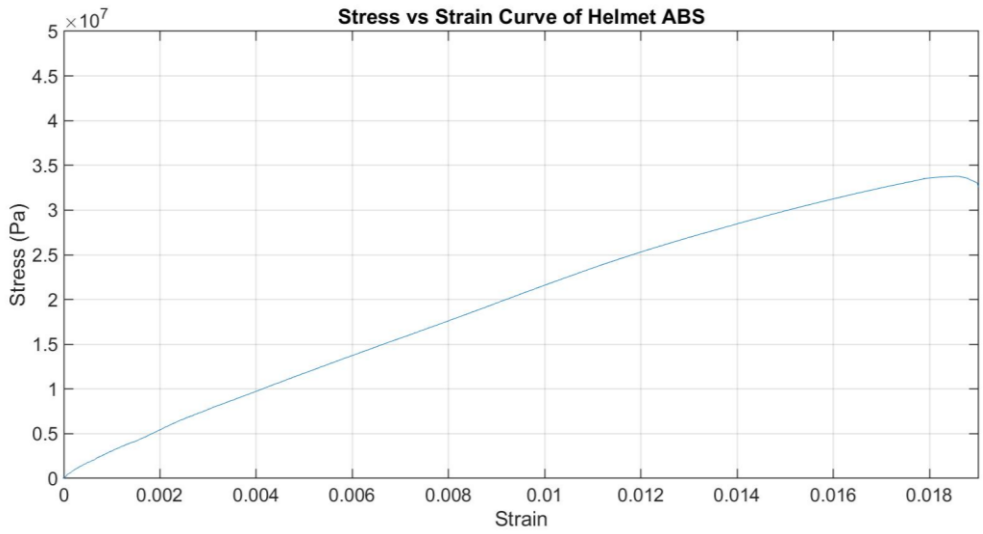

Figure 3.19: Stress- Strain curve of an ABS sample from Rawling's baseball helmet.

3.4.3 Assembly and analysis step

After the material properties were defined and the components modeled, the head form, helmet, and four conformal elements were assembled together as shown in Figure 3.20. The top surfaces of the conformal elements were oriented tangential to the surface of

the helmet shell, and the head form was placed in contact with and tangential to the bottom surface of the conformal elements. Contact between elements was prevented by maintaining sufficient spacing between elements.

For the analysis ABAQUS Explicit was used. The ABAQUS explicit simulation is well suited for brief dynamic simulations such as drop testing and crash tests. In this case the simulation was executed with 0.03 seconds as the impact simulation time. This time was obtained from acceleration versus time data from an actual test for a drop height of 12 inches, as documented in Figure 3.21. As was the case with quasi-static analysis, non-linear geometry was used to model the large deformations expected in the elements.

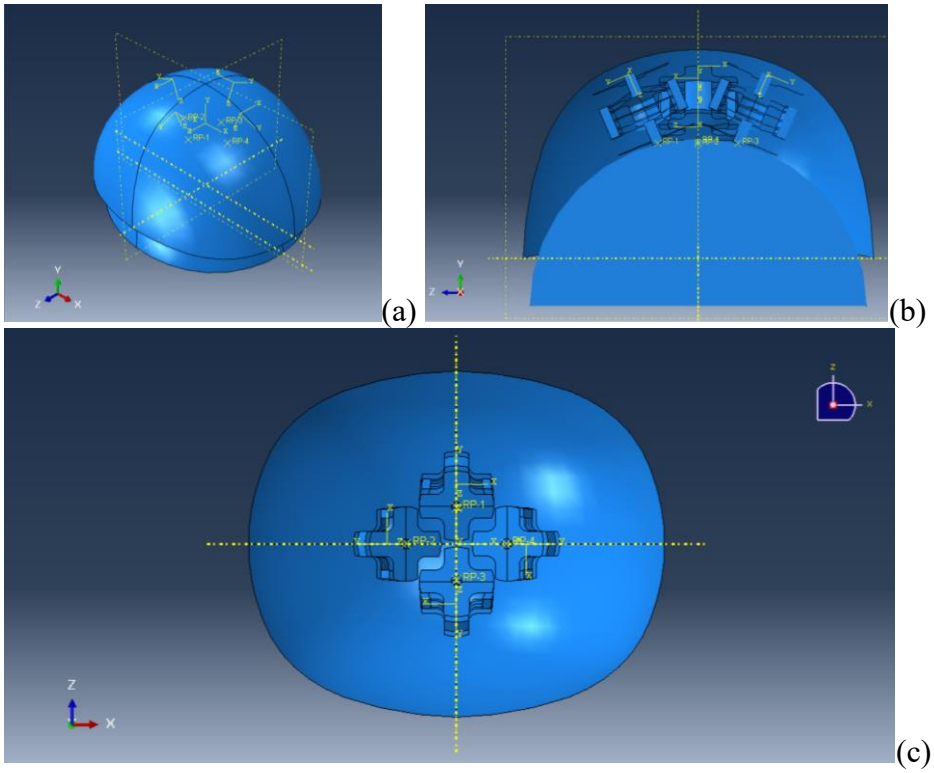

Figure 3.20: Assembly of the conformal elements, head form and helmet shell- (a) Isometric view of the assembly, (b) Section View, (c) Elements positioned on the helmet shell.

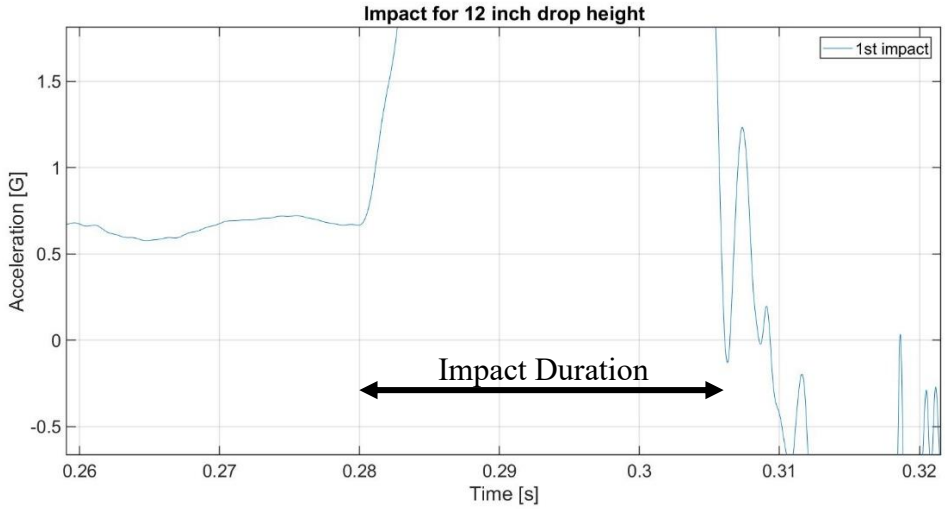

Figure 3.21: Time duration of impact.

The output database was configured to report the acceleration of a point at the center of the flat surface of the modeled head form as shown in Figure 3.22.

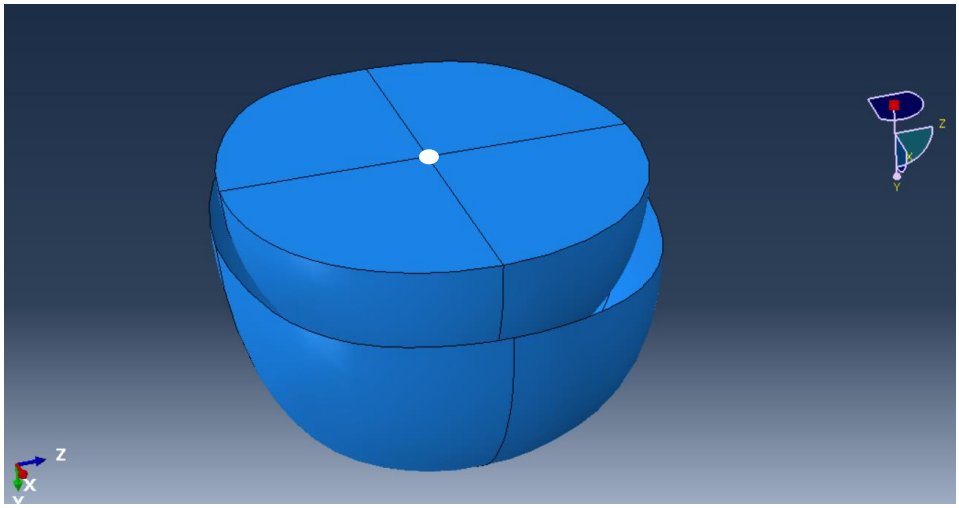

Figure 3.22: Reference point (in white) for which acceleration data was reported.

3.4.4 Loading, interaction and boundary conditions

The ‘General Contact’ option was chosen for defining all interactions during the analysis. This option allows for simplification of the interactions between different surfaces with very few restrictions on the type of surfaces involved. In ABAQUS explicit, it is recommended to use this option to define interactions rather than using other options in which all possible interactions for every surface must be specifically defined. Any error in such definitions can lead to incorrect results.

A combined non-structural mass of 8.5 kg was added to the helmet additionally to simulate the weight of the hardware of the test rig and was distributed evenly throughout the volume. A pre-defined velocity field of 2.4 m/s was prescribed to the whole model in the Y direction. This velocity was defined to simulate a mass of 8.5 kg falling from a height of 12 inches, as measured by a velocity sensor during a representative test.

Boundary conditions were also defined for the components. For each of the conformal elements, local coordinate systems were defined with the Z axes along the vertical axis of the elements as shown in Figure 3.23.

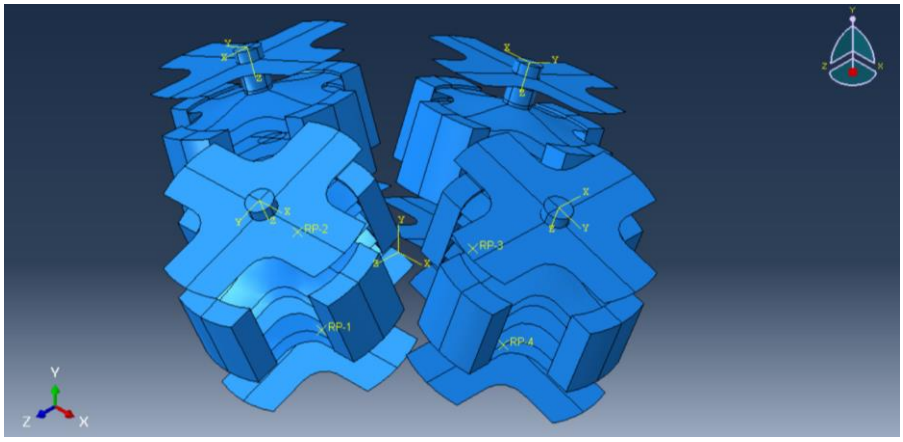

Figure 3.23: Local coordinate definition for each of the conformal elements with Z axes along the vertical axis of the elements.

Next, pinned boundary conditions were applied in the X and Y direction of the local coordinate system on the bottom surfaces of each of these elements as shown in Figure 3.24. This boundary condition simulates the effect of having the bases of conformal elements fixed to the inside of the helmet shell as would be the case during physical impact testing of these elements while allowing for free displacement in the Z direction.

Boundary conditions were also applied on the helmet shell in order to enable just one degree of freedom to simulate a one-dimensional impact. The bottom most point of the helmet shell was pinned to remove all the degrees of freedom except in the vertical direction as shown in Figure 3.25. Another boundary condition was specified on the same point of the model in which the velocity of the point reduced from 2.40 m/s to 0 m/s in 0.03 seconds in order to simulate the impact. This impact duration was estimated from the data obtained from actual drop test as shown in Figure 3.21.

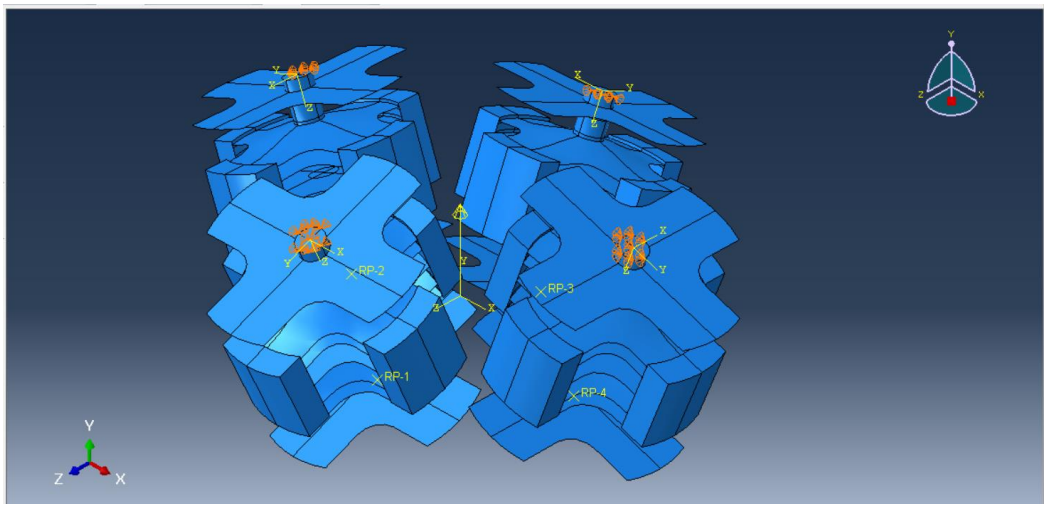

Figure 3.24: Pinned boundary condition on the bottom surface of the conformal elements.

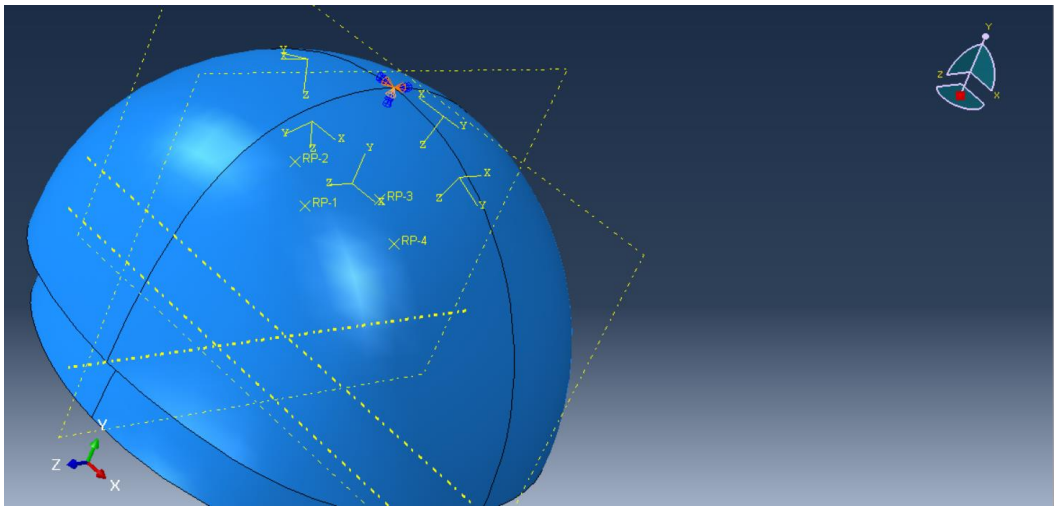

Figure 3.25: Pinned boundary condition on the apex point of the helmet.

3.4.5 Meshing

As was the case with quasi-static modelling, a combination of shell and solid elements was used in the assembly. Hence, those elements were meshed separately. The conformal elements were meshed as described for the quasi-static testing. The element size for the conformal elements was kept the same, i.e. 0.5 mm. For the head form, explicit, linear, hexagonal, 3D stress element-C38DR meshing element with reduced integration and hourglass control was used. The helmet shell was modeled with S4R elements, which are 4-node doubly curved shell elements with linear quadrilateral meshing and reduced integration and hourglass control.

The global element size for the head form and the helmet was specified to be 5 mm each. Initially, the element size for both the head form and the helmet was 10 mm. The element sizes for the head form and the helmet were refined till the results converged.

Test	Head form mesh element size (mm)	Helmet mesh element size (mm)	Impact Acceleration (g)
Trial 1	10	10	18.3918
Trial 2	10	8	18.3381
Trial 3	8	8	18.1461
Trial 4	8	5	18.2242
Trial 5	8	2	18.4595
Trial 6	5	5	18.5276
Trial 7	5	2	18.4965

Table 3.2: FEA results of impact simulation from 6 inches drop height for different mesh sizes.

The results obtained for different mesh element sizes for impact from drop height of 6 inches are tabulated in Table 3.2. The results converged around element size of 5 mm each for the head form and the helmet. The acceleration versus time curves for different element sizes is shown in Figure 3.26. Figure 3.27 shows the meshed assembly.

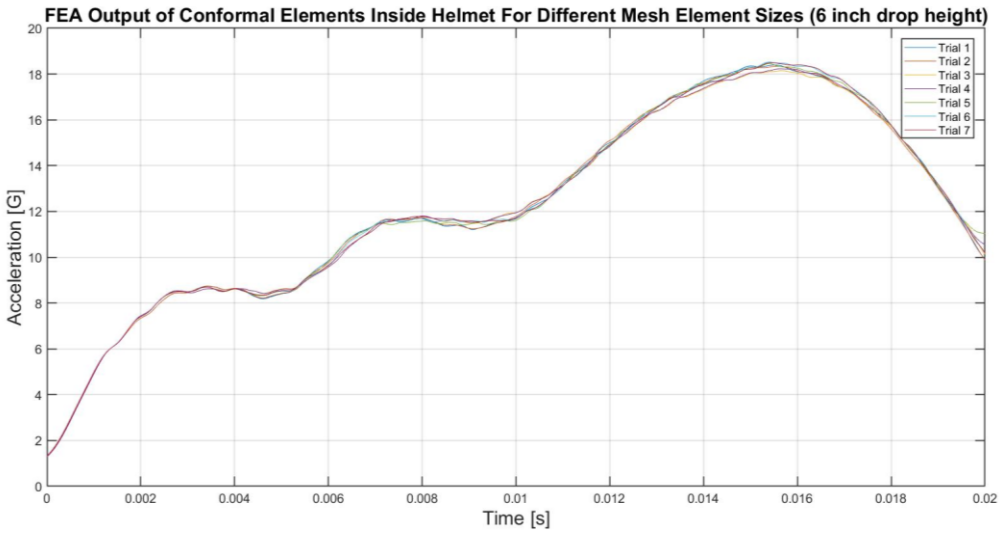

Figure 3.26: Acceleration versus time curves for different mesh sizes.

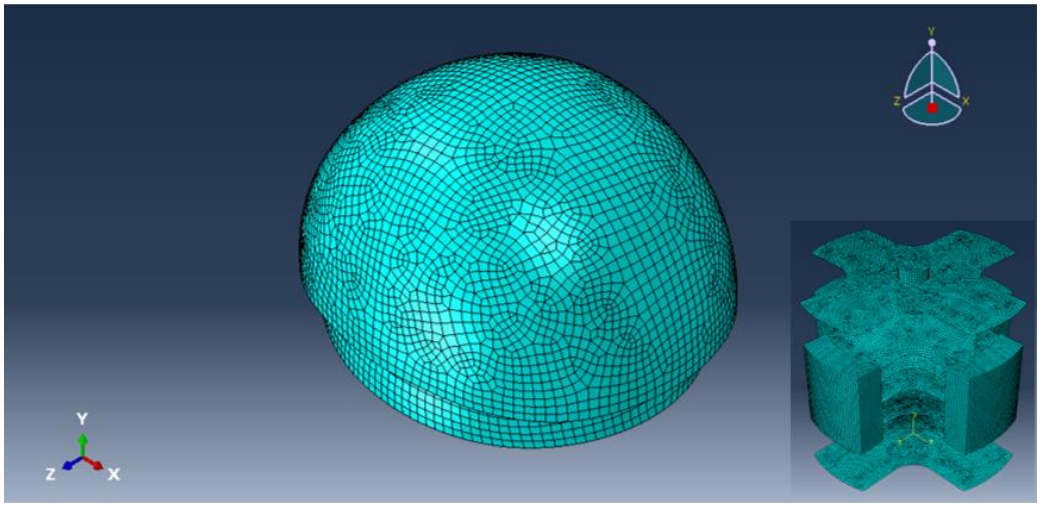

Figure 3.27: Meshed head form and helmet. Inset: Meshed conformal elements.

3.4.6 FEA results from impact loading.

After assembling the components and defining the interactions, loads and boundary conditions, the model was submitted for analysis. The data obtained was filtered using

Butterworth filter plugin available in ABAQUS with a cut off frequency of 500 Hz. The resulting acceleration versus time curve is shown in Figure 3.28.

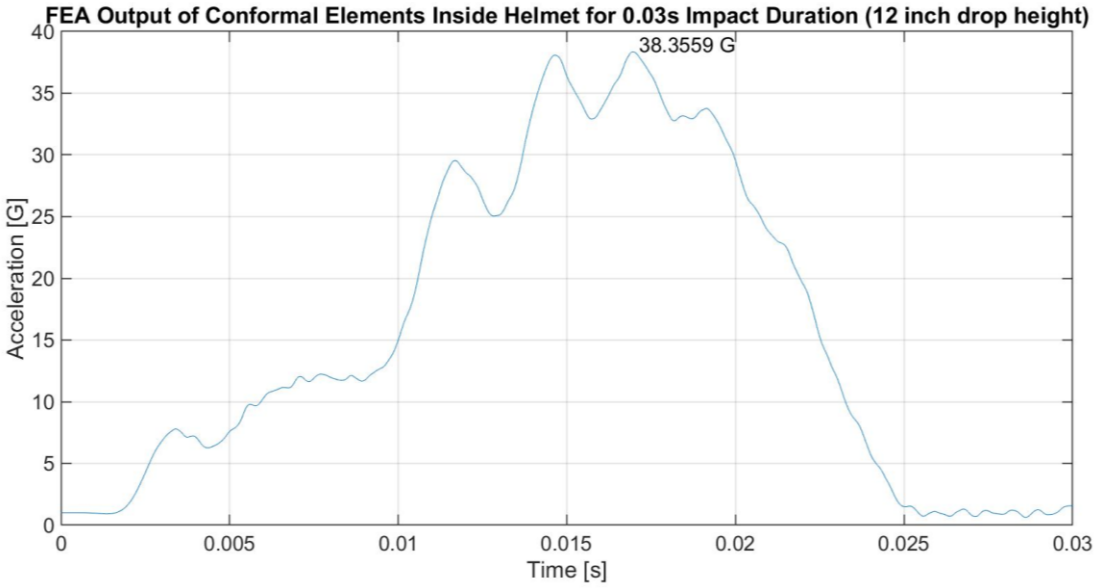

Figure 3.28: Acceleration versus time curve for impact FEA analysis – 12 inch drop height.

The maximum impact magnitude predicted through FEA for a 12 inch drop height with conformal elements placed inside the helmet was 38.36 g. The buckling modes are shown in Figure 3.29.

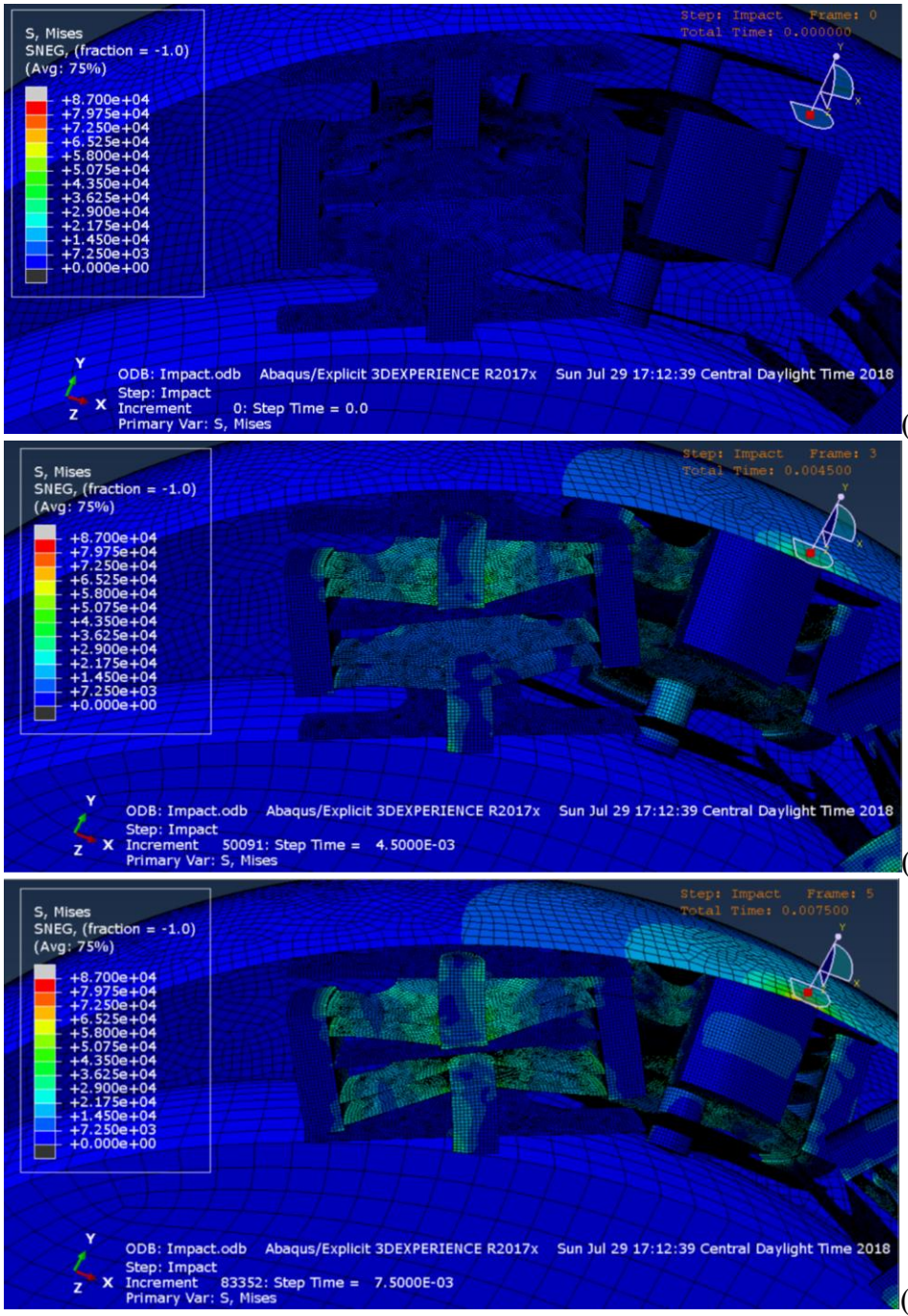

Figure 3.29: Conformal elements in (a) Stage 1 – Initial uncompressed stage, (b) Stage 2 – Thinner beams snap through, (c) Stage 3 – Fully compressed state.

During the FEA simulation very high values of stress were reported. The stress contour in the element was redefined to show the regions where stress has exceeded the yield stress in black. The resulting stress contour is shown in Figure 3.30.

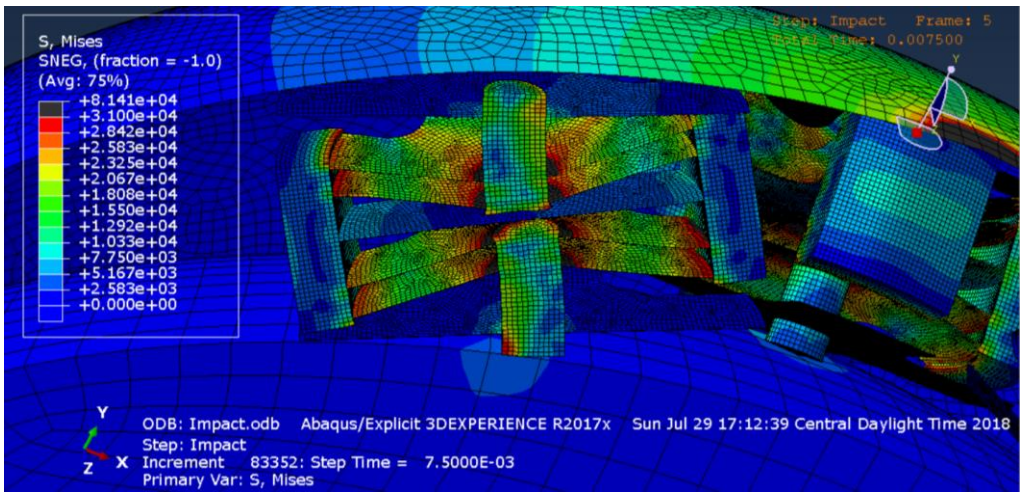

Figure 3.30: Dark regions depicting stress values higher than yield stress.

As can be seen in Figure 3.30, the regions of high stress concentration are near the edges where shell to solid coupling has been defined. As discussed in Section 3.3.5 the stress concentration is caused due to sharp corners. Chamfers and fillets have been provided to relieve stress from these areas.

A similar impact testing simulation was conducted for a 24 inch drop height. The boundary condition on the bottom most point of the helmet shell was specified in which the velocity of the point reduced from 3.25 m/s to 0 m/s in 0.015 seconds. This duration was estimated from the data obtained from actual drop tests. The resulting acceleration versus time graph is shown in Figure 3.31. The maximum impact magnitude predicted through FEA for a 24 inch drop height with conformal elements placed inside the helmet was 82.39 g.

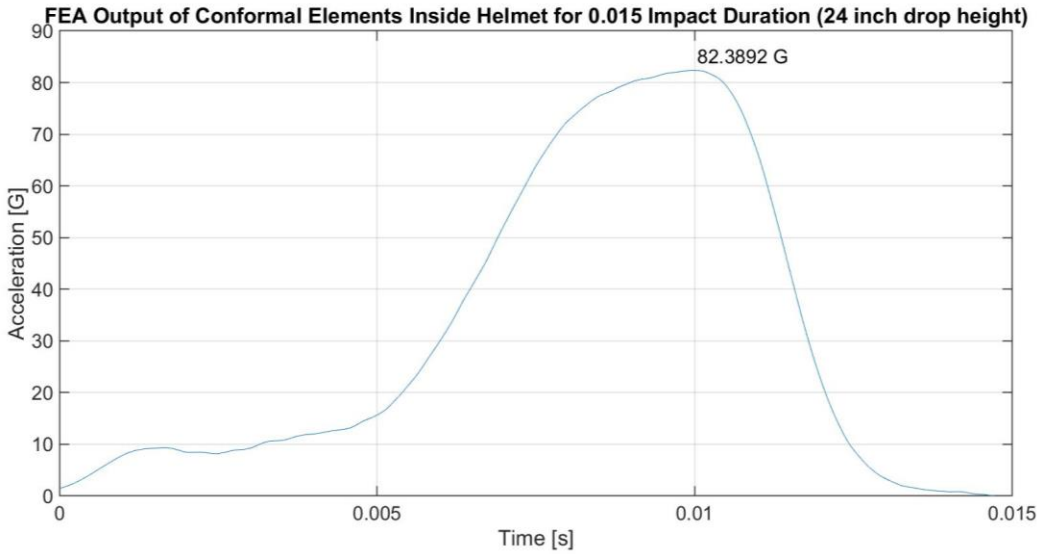

Figure 3.31: Acceleration versus time curve for impact FEA analysis – 24 inch drop height.

3.5 SUMMARY

In this chapter the FEA of the conformal elements under quasi-static and impact loading conditions was discussed. This chapter describes the modelling and definition of material properties, interactions, boundary conditions, loading, and constraints. The analysis procedure is also discussed extensively. As predicted during the design phase, two distinct force thresholds were obtained for the conformal elements. The FEA prediction of force threshold after quasi-static testing was 189.08 N and 246.47 N for thinner and thicker beams respectively. For impact FEA simulation, the maximum impact magnitude with the conformal elements placed inside the helmet for a drop height of 12 inches was 38.36 g and for a drop height of 24 inches, it was 82.39 g. In the next chapter physical tests of the helmet assembly are discussed, and the results of FEA and actual tests are compared.

Chapter 4: Experimental Testing

4.1 Introduction

The conformal elements were subjected to quasi-static and dynamic physical testing. The conformal elements were then placed inside of an actual baseball helmet, backed with the additively manufactured head form described in Chapter 3, and tested under dynamic conditions. Conventional padding was also tested under the same loading conditions. The performance of the conformal elements was compared to that of conventional padding and to the results of the FEA analysis. The experimental procedure is described first, followed by the results and comparisons.

4.2 Quasi-Static Testing

4.2.1 Experimental procedure

For the purpose of determining the force threshold of the manufactured conformal elements, they were subjected to quasi-static testing using an MTS test frame (as shown in Figure 4.1). The four elements were tested individually. The displacement load rate was 5 mm/min and the displacement limit was set at 13 mm. The displacement limit was set after taking measurements of the manufactured sample and calculating the maximum allowable displacement for the beams. The zero displacement of the crosshead was set when it reached the top of the conformal element without applying any load on the conformal elements. The elements were compressed and then unloaded until the crosshead returned to its starting position.

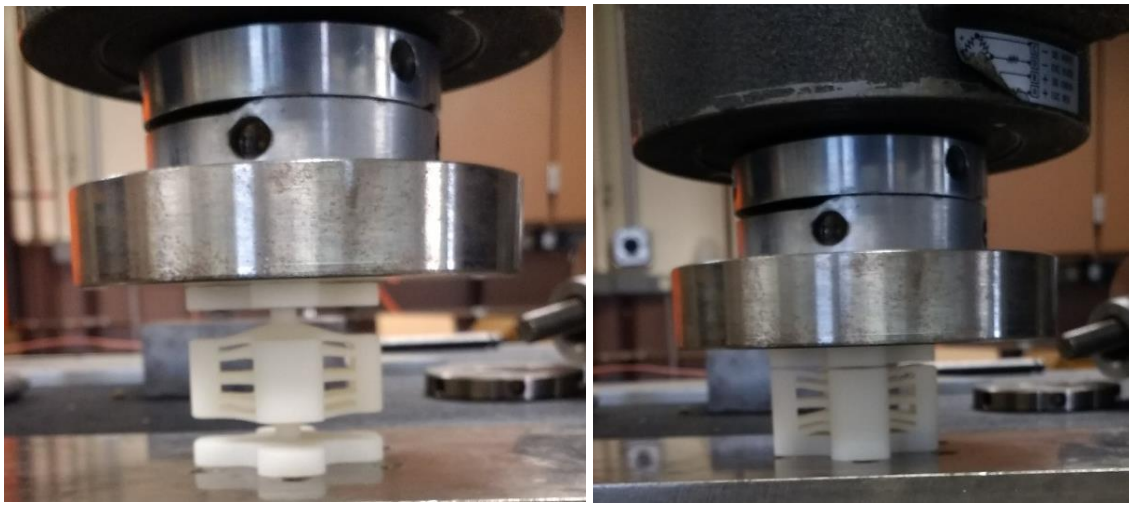

Figure 4.1: Quasi-static testing. Initial state of the conformal element (left) and fully compressed state (right).

4.2.2 Results of quasi-static testing

The force-displacement curves obtained from the testing are shown in Figure 4.2. The force threshold for thinner beams was found to be in the range of 150N to 200 N while that for thicker beams was in the range of 250N to 300N. The variation in force threshold can be attributed to the observed variance in actual dimensions of the manufactured conformal elements as shown in Table 4.1.

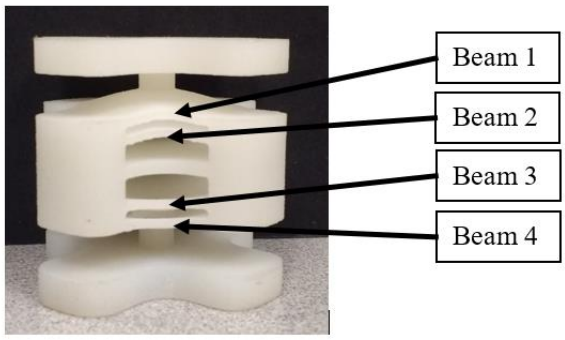

Figure 4.2: The thicknesses of the beams were measured and recorded in Table 4.1.

Element	Beam 1 Thickness (mm)	Beam 2 Thickness (mm)	Beam 3 Thickness (mm)	Beam 4 Thickness (mm)
1	1.39	1.39	1.54	1.56
	1.41	1.41	1.54	1.52
	1.40	1.41	1.53	1.54
2	1.39	1.42	1.54	1.52
	1.40	1.41	1.52	1.54
	1.40	1.40	1.55	1.57
3	1.41	1.40	1.52	1.57
	1.40	1.41	1.53	1.57
	1.39	1.38	1.53	1.54
4	1.42	1.40	1.55	1.51
	1.39	1.40	1.50	1.53
	1.39	1.41	1.49	1.52

Table 4.1: As measured beam thickness of conformal elements.

Dimensions were taken at three different points on each beam for every element. Another important observation was that, for each of the elements, the force threshold is higher for the first trial than for the second because minor plastic deformation is observed. Due to this plastic deformation, the overall height of the elements also decreased causing an initial ‘lag’ in the force displacement curve between the first and second trials of the quasi-static testing. This phenomenon was observed for previous design iterations of the conformal elements made of nylon 11, as well (Debeau *et al*., 2018). After the first compression, the force thresholds stabilize to a consistent value.

Another important aspect of the elements was that the thinner beams exhibited bi-stability, characterized by negative reaction force during the unloading stage, even though the Q factor was designed to be 2.33, which is less than the experimentally determined 2.71 threshold that marks the transition to bi-stability. However, this bi-stability behavior was not observed during impact testing. The elements regained their shape after the impacts.

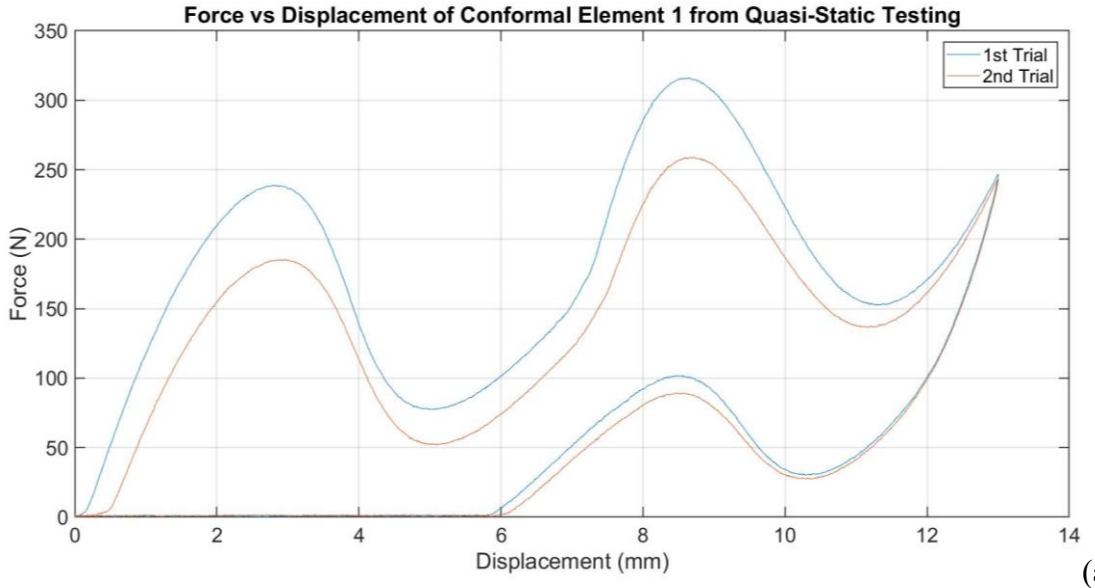

(a)

Figure 4.3: (a) Force versus displacement curves obtained from quasi-static testing of conformal element 1.

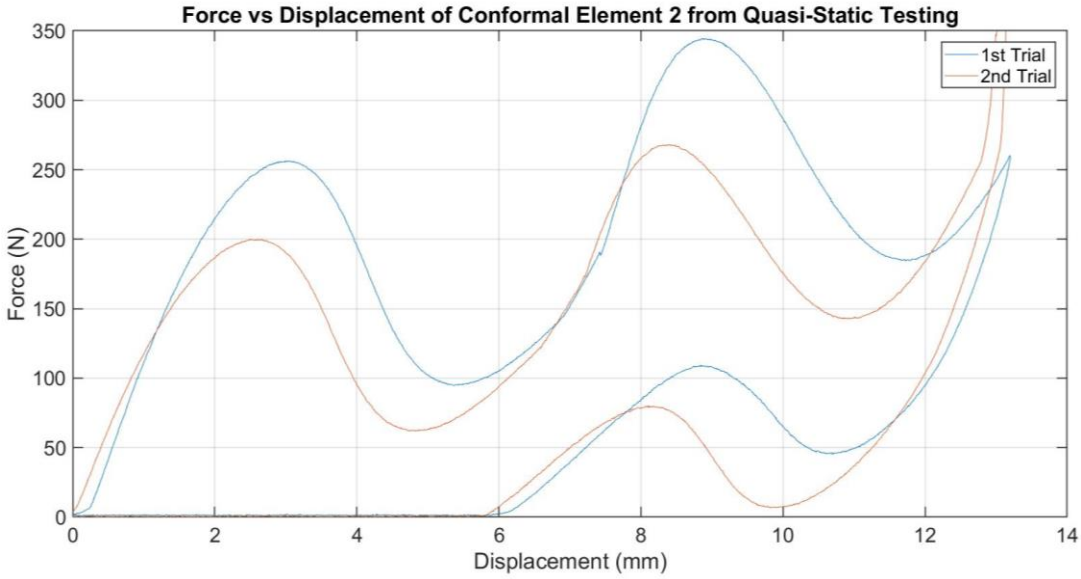

(b)

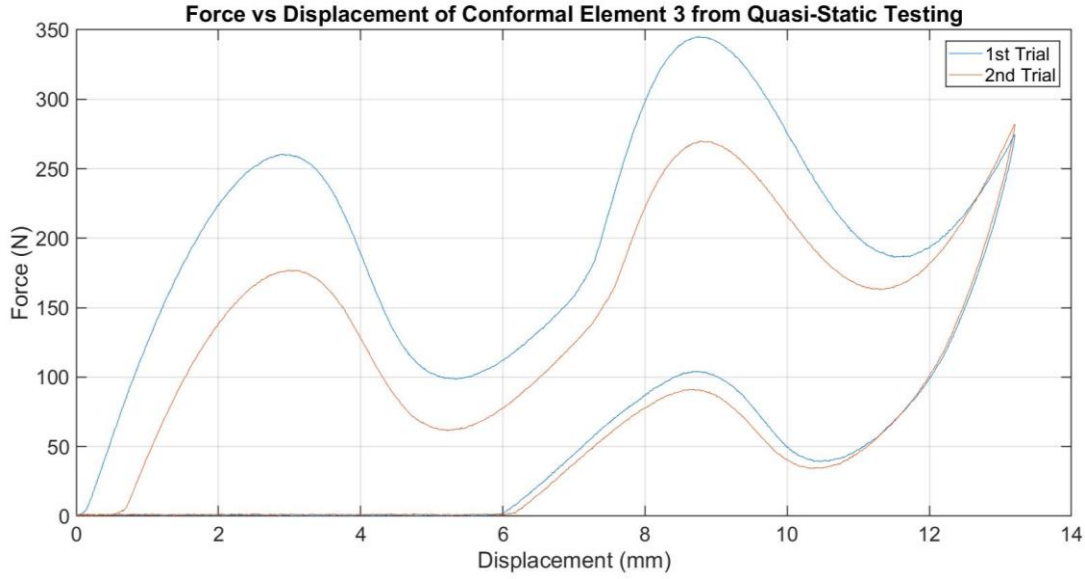

(c)

Figure 4.3 (contd.): (b) & (c) Force versus displacement curves obtained from quasi-static testing of conformal elements 2 and 3.

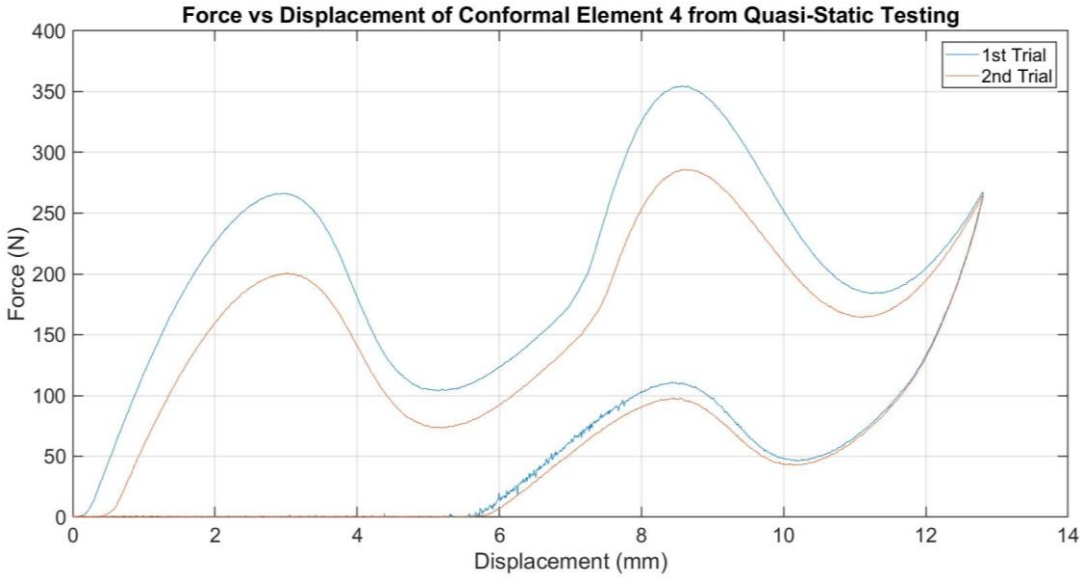

(d)

Figure 4.3 (contd.): (d) Force versus displacement curves obtained from quasi-static testing of conformal element 4.

For the finite element analysis, the dimensions of Conformal Element 1 were considered and the as-measured dimensions were input into the model. The force threshold prediction was 189.08 N and 246.47 N for thinner and thicker beams respectively, while the actual force threshold obtained was 184.93 N and 258.95 N. The FEA results obtained agree very closely to the actual results obtained. In the FEA analysis, the beams had a constant specified cross section, while in actual samples variances in the dimensions were observed, which might also have an impact on the difference in results obtained.

4.3 IMPACT TESTING

After quasi-static testing, the elements were subjected to impact testing. Two different kinds of impact testing were performed on the conformal element: independent testing of the elements themselves and assembled testing of the elements together with the

helmet and head form. Conventional padding was also subjected to equivalent impact tests, and the results were compared.

4.3.1 Conformal Elements versus Conventional Padding under Direct Impact

4.3.1.1 Experimental procedure

The impact testing was performed on a drop test rig. The drop test rig comprised of a carriage on which different masses could be attached. This carriage could slide freely in a vertical channel with the help of sliding bearings as shown in Figure 4.4. On the top of this carriage a single axis, PCB 352C03 accelerometer was attached to measure the impact acceleration. This accelerometer was connected to a NI-9234 input module on a DAQ chassis which could be connected to a computer. Data was collected with the help of MATLAB.

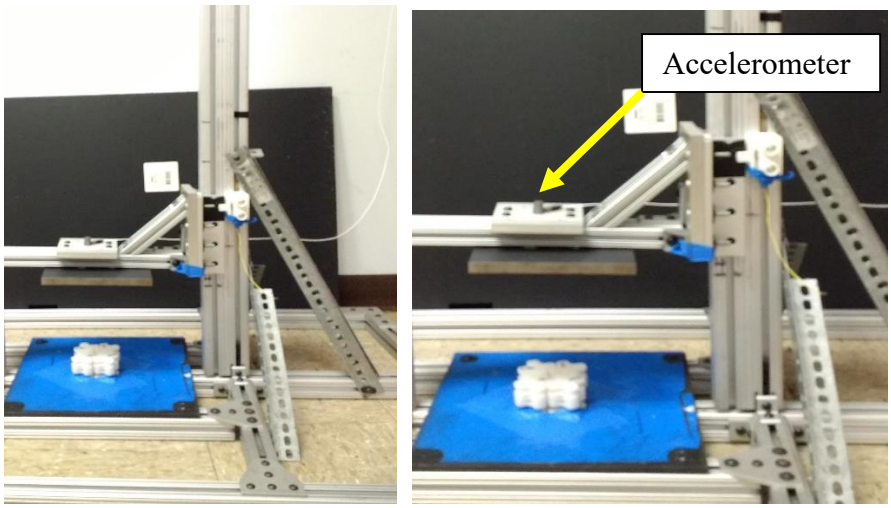

Figure 4.4: Drop test rig with accelerometer mounted on top of the carriage.

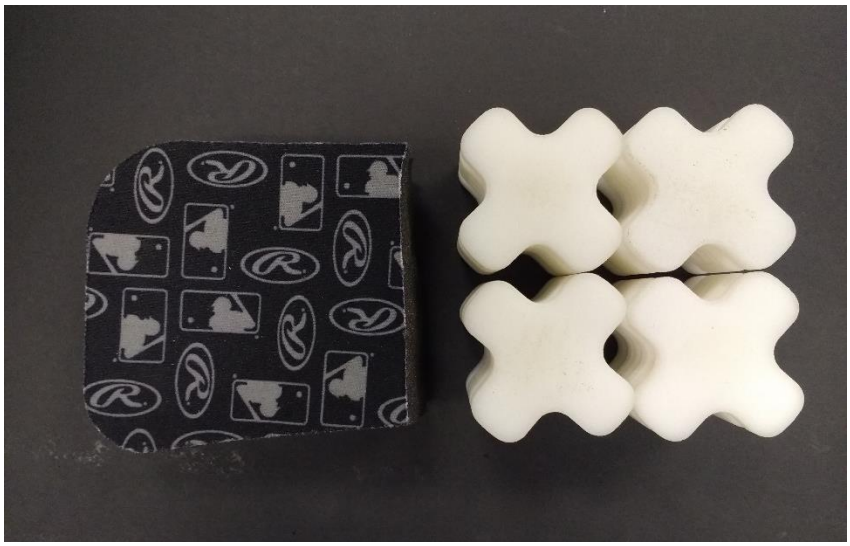

Figure 4.5: Baseball helmet foam and conformal elements used during testing.

In this test, a 5.5 kg combined mass of the entire carriage was allowed to fall from different heights on the impact absorbing elements. The elements were secured on the base of the drop test rig to prevent any undesirable movement of the elements during or after the impact. The performance of conformal elements and conventional baseball padding were tested for drop heights of three, six and nine inches. As described earlier, the elements were designed and checks were performed using FEA around a similar impact.

The baseball foam sample was taken from a Rawling's Velo baseball helmet. The foam was cut to have the same footprint area as four conformal elements tiled in parallel as shown in Figure 4.5. The foam sample was taken from the sides of the helmet since the foam on the side of the helmet was thicker than the foam at the top. The goal was to test baseball foam with a cross-sectional area and height as close as possible to that of the conformal elements. Datums were established at the uncompressed height of the foam and the conformal elements individually and heights of three, six, and nine inches above those datums were measured as drop heights for the falling arm.

4.3.1.2 Results

Three impact trials were completed for each element from each drop height to capture the repeatability of the tests. The impact acceleration versus time curves obtained from the trials are overlaid in the diagrams in Figure 4.6. The acceleration data has been filtered by a third order, low pass Butterworth filter with a cut off frequency of 500 Hz. The peak impact accelerations are presented in Table 4.2.

Drop Height (inches)	Range of peak impact acceleration for baseball foam (g)	Range of peak impact acceleration for conformal NS elements (g)
3	25 - 32	23 -25
6	60 - 63	24 - 26
9	82 - 84	28 - 30

Table 4.2: Performance comparison of baseball foam versus conformal elements under direct impact.

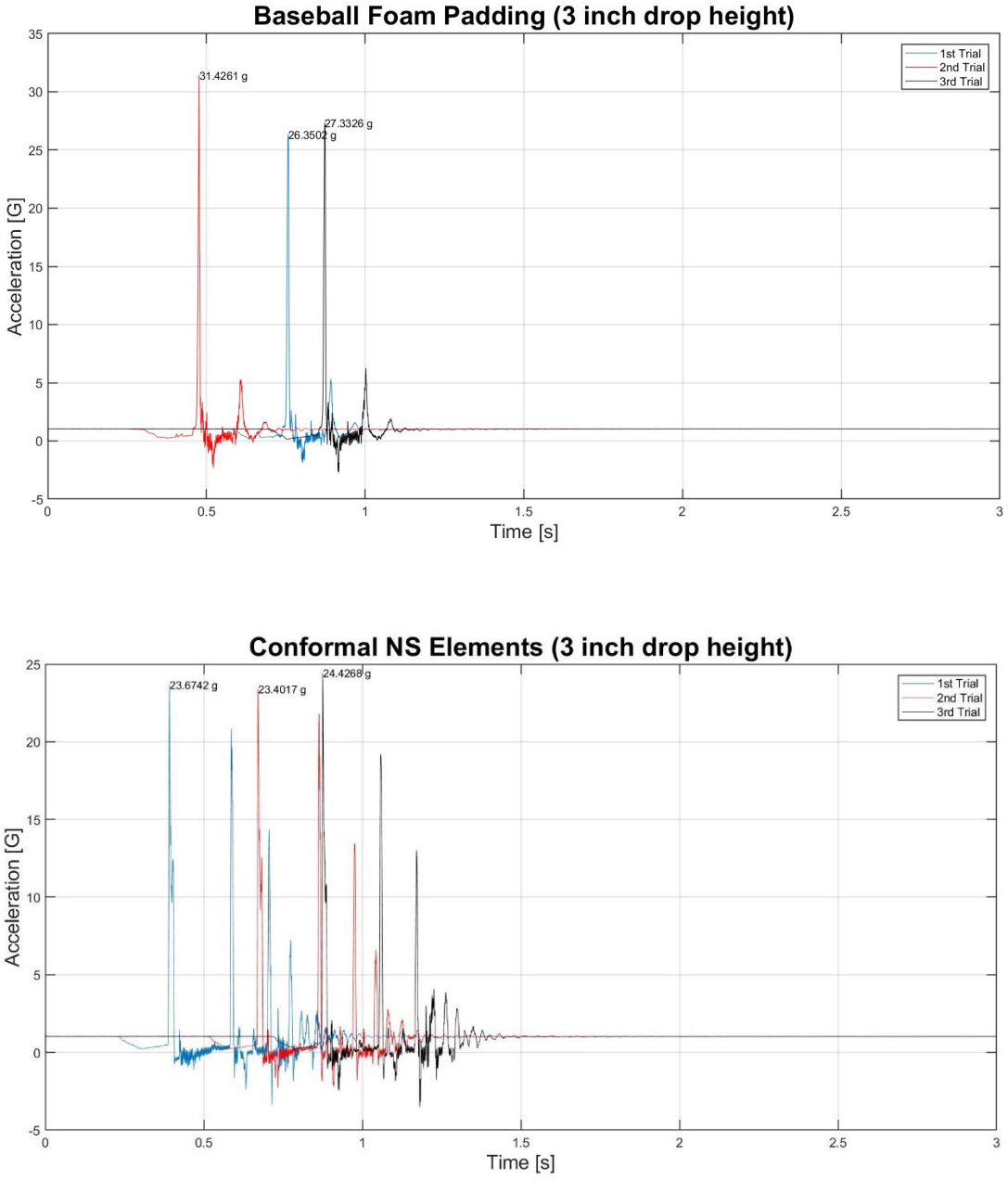

(a)

Figure 4.6: Acceleration versus time for conformal NS elements and baseball foam padding derived from experimental impact testing. Results for (a) 3 inch drop height.

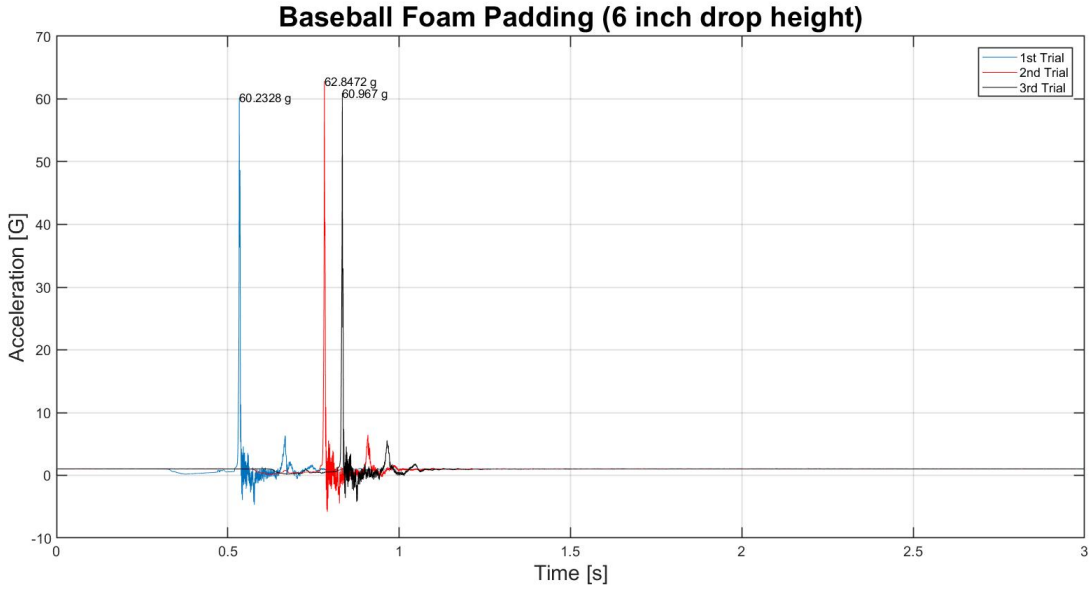

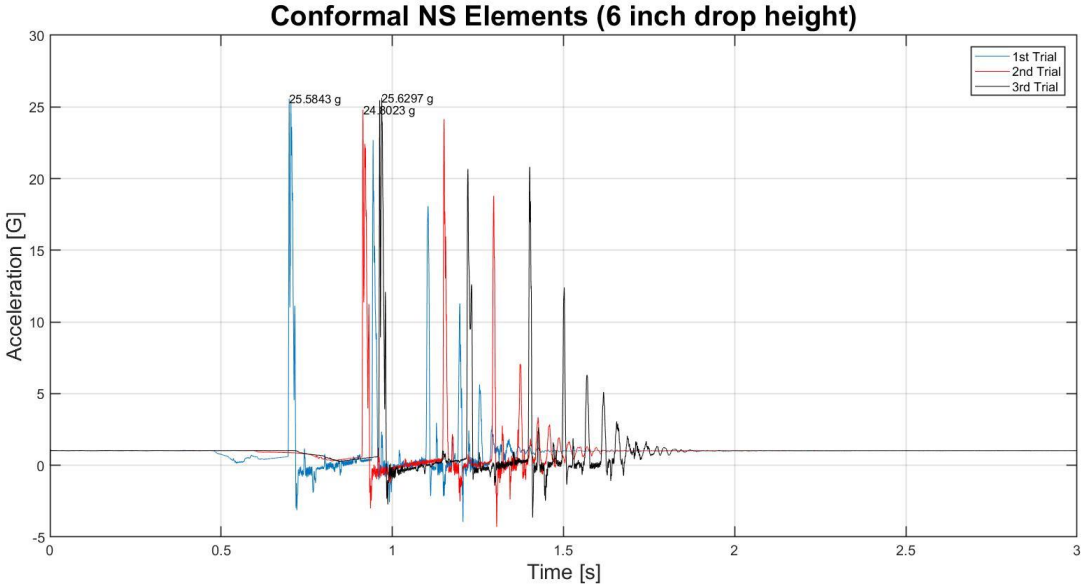

(b)

Figure 4.6 (contd.): Acceleration versus time for conformal NS elements and baseball foam padding derived from experimental impact testing. Results for (b) 6 inch drop height.

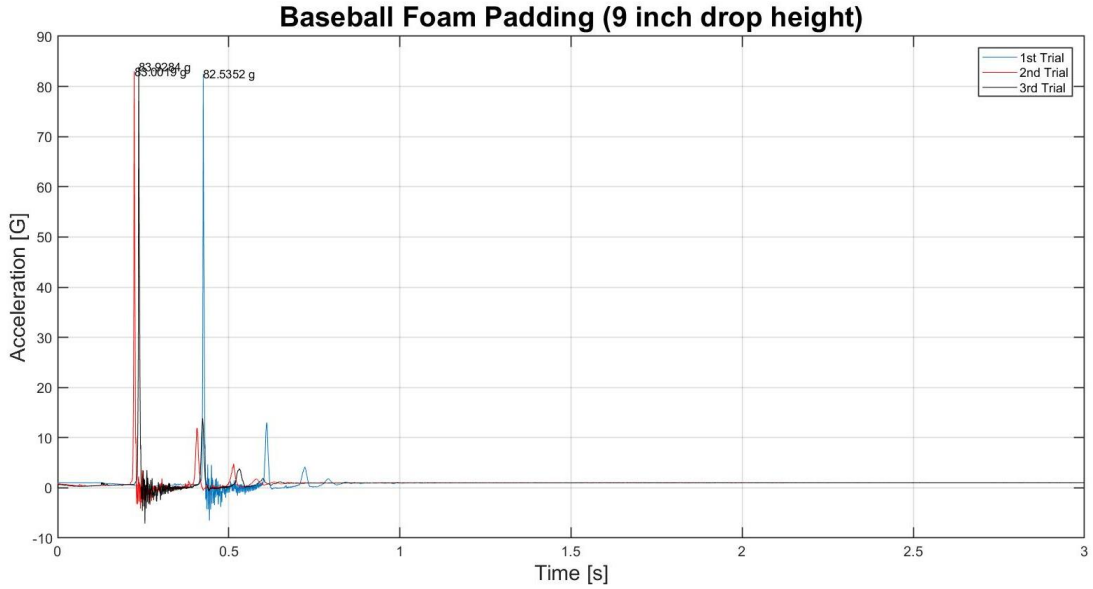

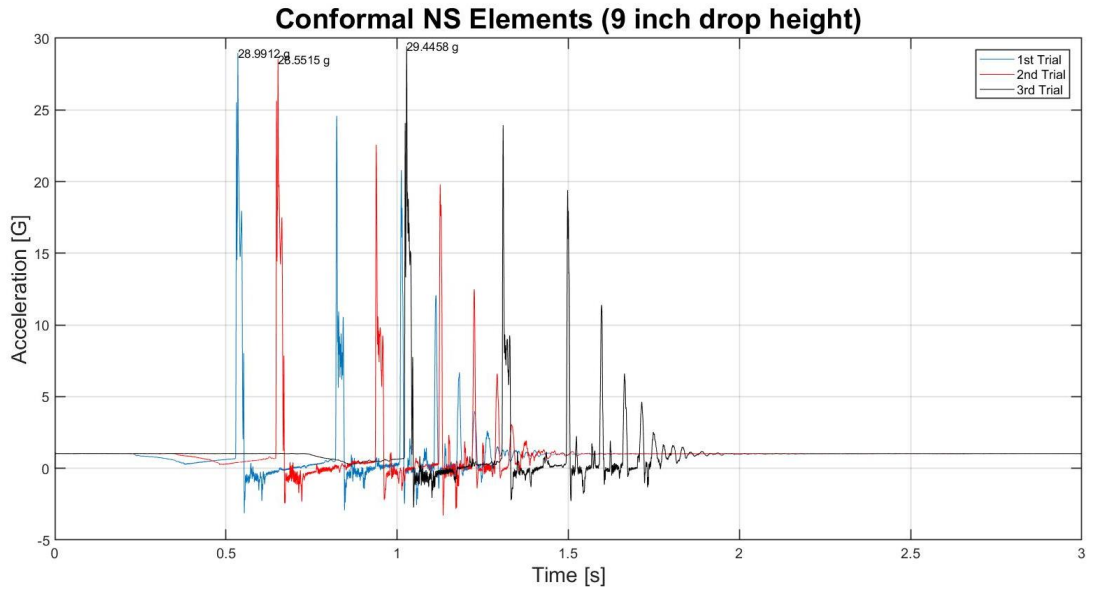

(c)

Figure 4.6 (contd.): Acceleration versus time for conformal NS elements and baseball foam padding derived from experimental impact testing. Results for (c) 9 inch drop height.

During the tests the carriage was lifted up to the specified height and held in position manually. Once the impact acceleration data collection started, the carriage was

let go and allowed to fall freely. Since it was a manual operation, the time when the carriage started to fall varied from trial to trial, which caused the difference in the times at which the peak accelerations occur.

As can be seen from the experimental data the conformal element performed better than the baseball foam padding for all drop heights. The impact was mitigated and thresholded at values of 23 g to 30 g for all drop heights. The baseball foam padding's acceleration was comparable to that of the conformal NS elements for the 3 inch drop height. For drop heights of 6 inches and 9 inches the impact acceleration increased to approximately 60 g and 80 g, respectively, while the impact acceleration for the conformal elements remained reasonably consistent in the range of 25 g to 28 g. This comparison shows that the pre-curved beams engaged without bottoming out for both lower and higher impacts, and the design was very effective in mitigating the impacts. These conformal elements outperformed the initial design of conformal elements which had a constant force threshold and were discussed in Section 2.4.1. The impact acceleration versus time graphs for the initial design of conformal elements are shown in Figure 4.7. The performance of both kinds of conformal elements were similar for drop heights of 3 inches and 6 inches, but for 9 inches the impact acceleration for the initial design was between 50 g to 60 g and much higher than that of the redesigned conformal element.

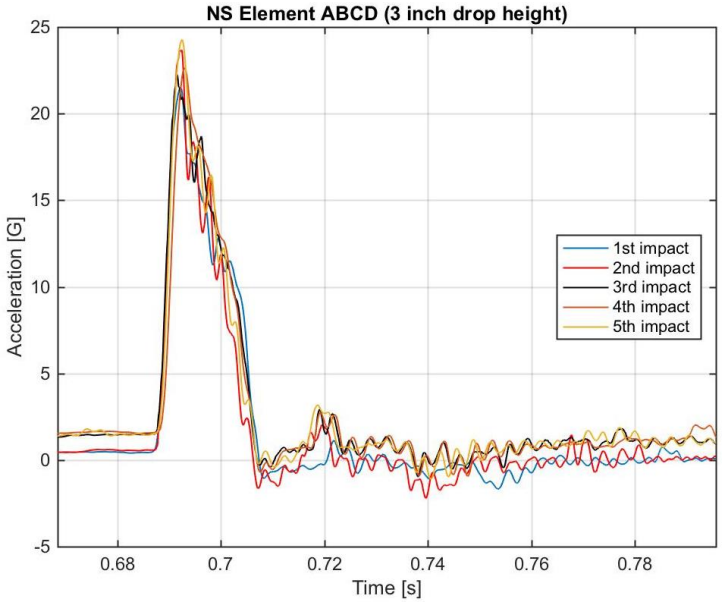

(a)

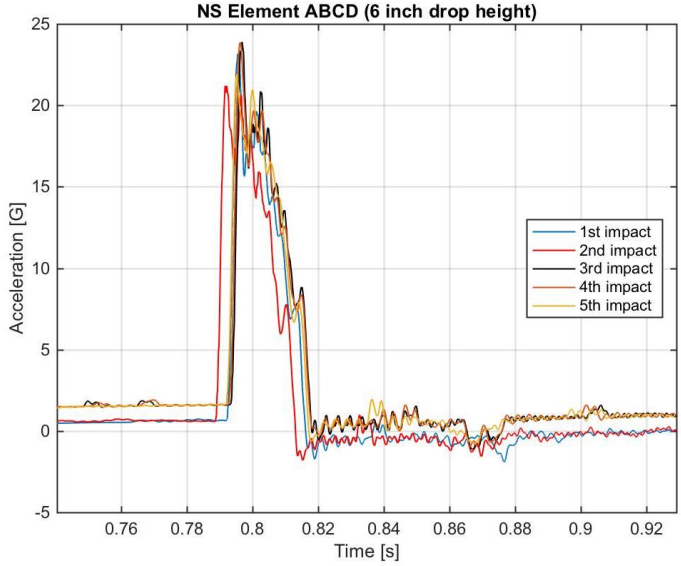

(b)

Figure 4.7: Acceleration versus time for initial design of conformal NS elements derived from experimental impact testing. Results for (a) 3 inch drop height, (b) 6 inch drop height.

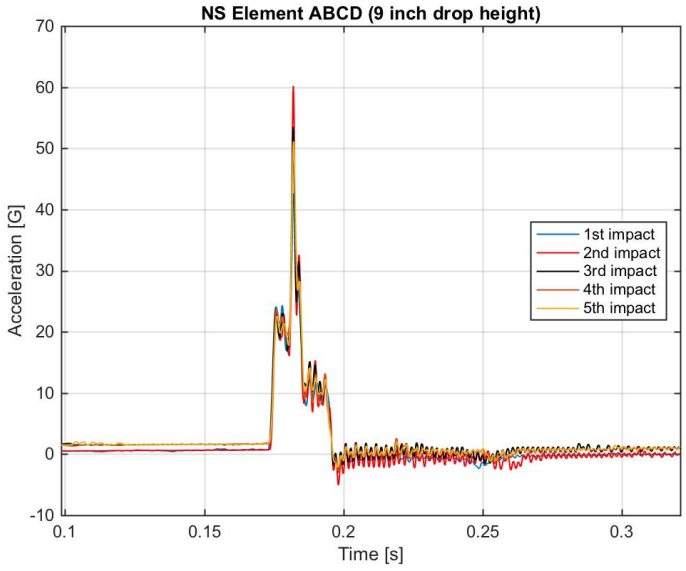

(c)

Figure 4.7 (contd.): Acceleration versus time for initial design of conformal NS elements derived from experimental impact testing. Results for (c) 9 inch drop height.

4.3.2 Conformal Elements versus Conventional Padding inside Helmet

4.3.2.1 Experimental procedure

Impact testing was also conducted with the conformal elements inside the helmet, and their performance was compared to that of conventional padding. A Rawling's Velo baseball helmet was modified for the test. The padding at the top of the helmet was removed and conformal elements were secured in the opening as shown in Figure 4.8 (a). Subsequently, the conformal elements were replaced with a baseball helmet foam sample having the same footprint as that of the conformal elements (and the same baseball foam used during direct impact testing discussed earlier) as shown in Figure 4.8 (b).


(a)

(b)

Figure 4.8: (a) Conformal Elements, (b) Foam Sample placed inside the helmet shell for impact testing.

As described in Section 3.4.1 and Section 3.4.2, the manufactured head form was placed inside the helmet and an additional mass was added to the head form to bring the overall mass of the entire falling assembly, including the hardware attached to the arm, to a total of 8.5 kg. The assembly with conformal elements and then baseball foam padding was subjected to drop tests from heights of 3 inches, 6 inches, 12 inches and 24 inches using the instrumented drop test rig discussed earlier, and their performance was compared. The impact magnitude was recorded using the accelerometer mounted on top of the falling arm. A datum was established at the uncompressed height of each assembly (i.e., with conformal elements or baseball foam), and the drop heights were measured from the respective datum.

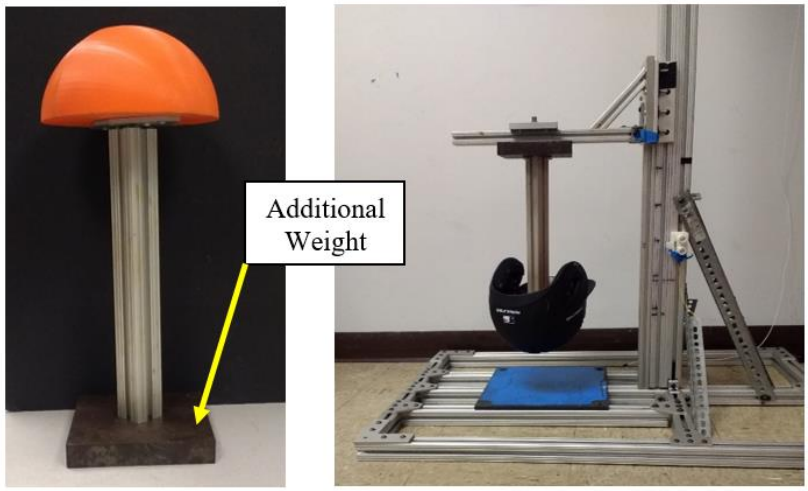

Figure 4.9: Left- The modeled head form, Right- The testing set up.

4.3.2.2 Results

Multiple trials were conducted for each assembly for each drop height to ensure repeatability. The acceleration versus time curves are shown in Figure 4.10.

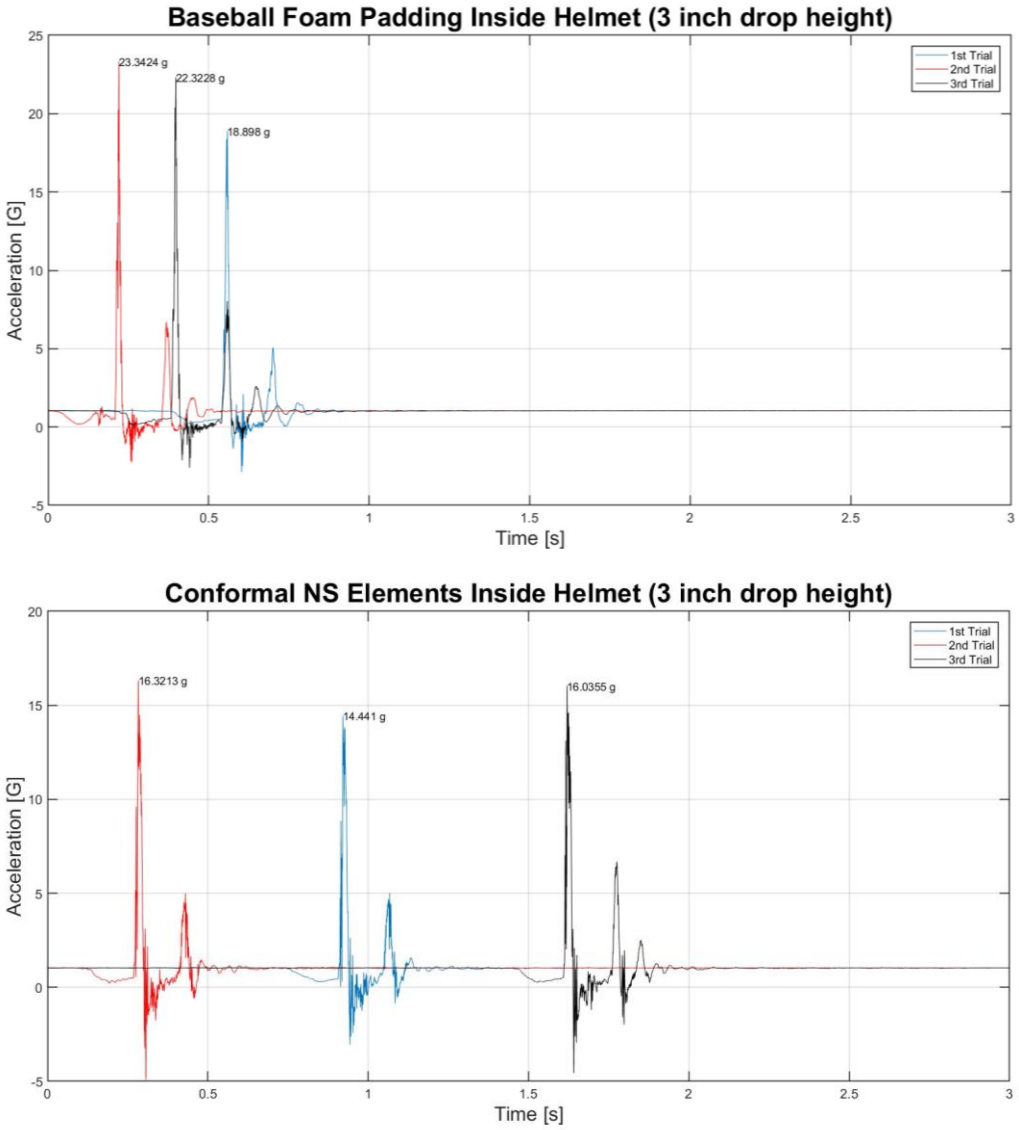

(a)

Figure 4.10: Impact acceleration versus time curves obtained for baseball foam and conformal NS elements placed inside the helmet for drop height of (a) 3 inches

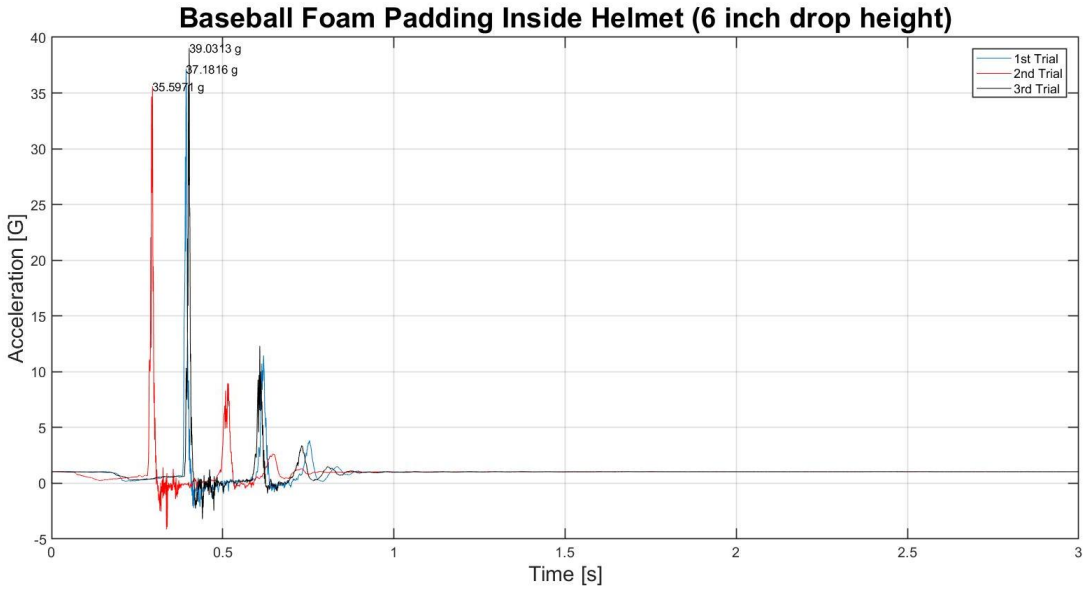

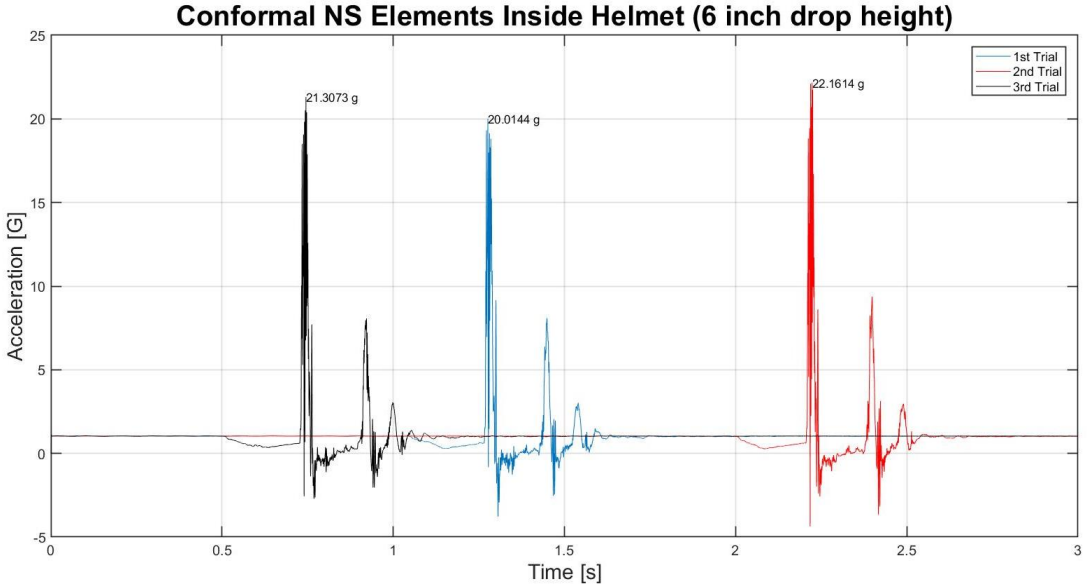

(b)

Figure 4.10 (contd.): Impact acceleration versus time curves obtained for baseball foam and conformal NS elements placed inside the helmet for drop height of (b) 6 inches

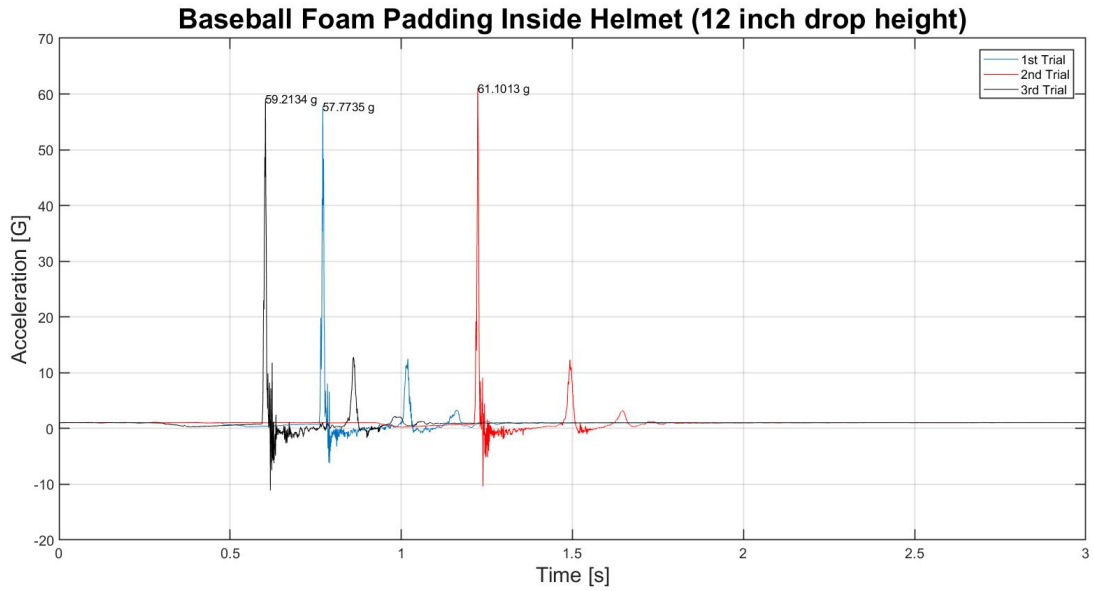

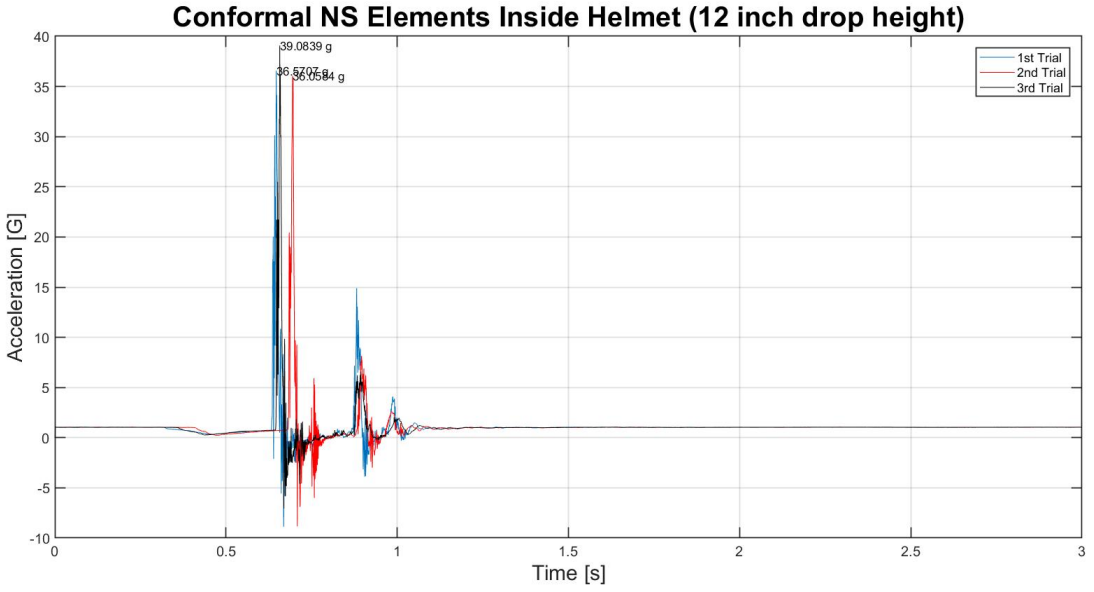

(c)

Figure 4.10 (contd.): Impact acceleration versus time curves obtained for baseball foam and conformal NS elements placed inside the helmet for drop height of (c) 12 inches

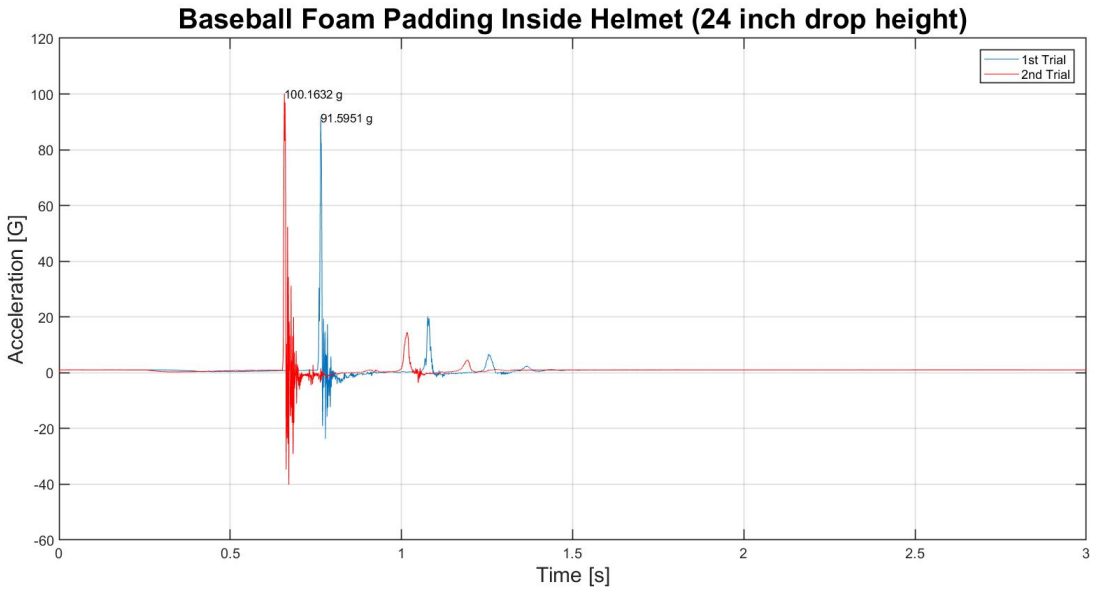

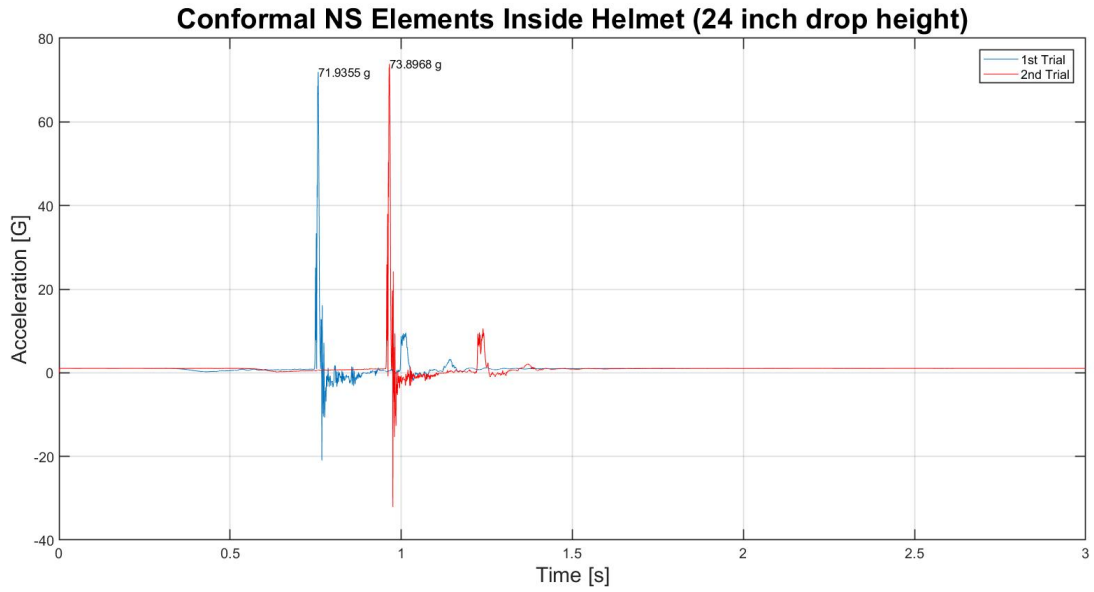

(d)

Figure 4.10 (contd.): Impact acceleration versus time curves obtained for baseball foam and conformal NS elements placed inside the helmet for drop height of (d) 24 inches.

As expected, the conformal elements outperformed the baseball foam. The conformal NS elements were able to mitigate low as well as high impacts. A comparison of the peak impact accelerations is summarized in Table 4.3

Drop Ht (in)	Peak acceleration for baseball foam (g)	Peak acceleration for conformal elements (g)	FEA prediction for conformal elements (g)
3	23	16	11.5
6	39	22	18.5
12	61	39	38.5
24	100	74	82.0

Table 4.3: Peak impact acceleration of baseball foam versus conformal elements.

For smaller impacts, i.e. for drop height of 3 inches, the impact acceleration for conformal elements was in the range of 14 g to 17 g while that for baseball helmet foam was 18 g to 25 g. This shows that the beams engaged and snapped through. For 6 inch drop, the impact acceleration for conformal elements was again thresholded at 20 g to 23 g, while for the foam it was 35 g to 40 g. The conformal elements performed better for higher impacts as well. For drop height of 12 inches and 24 inches, the impact acceleration for conformal elements was measured in the range of 35 g to 40 g and 70 g to 75 g respectively, in comparison to the foam padding for which the corresponding impact acceleration was in the range of 57 g to 62 g and 90 g to 100 g respectively.

For drop heights of 24 inches, high values of impact acceleration were obtained which shows that the beams snapped through completely and the elements bottomed out during the impact, but they were still able to absorb a lot of energy. The conformal

elements were able to significantly mitigate the impact, and their performance was consistent and repeatable.

For the direct impact testing discussed earlier on the conformal elements with a mass of 5.5 kg, the impact acceleration for drop height of 3 inches and 6 inches were higher (23 g to 25 g for 3 inches and 24 g to 26 g for 6 inches) as compared to impact testing done with the conformal elements inside of the helmet for the same drop heights even though the falling mass was higher (8.5 kg). This can be attributed to the helmet shell, which most likely absorbed a significant amount of impact energy.

The impact for drop height of 12 inches was simulated in FEA which was discussed in the previous chapter. The impact velocity for the 12 inch drop height was ascertained to be 2.4 m/s which was input in the model. The maximum impact magnitude from FEA analysis obtained was 38.36 g. The impact acceleration from actual testing was approximately 36 g to 38 g. Similarly, the FEA simulation for drop height of 24 inches predicted an impact acceleration of 82.39 g, while the value obtained from actual testing was around 70 g to 75 g. The impact accelerations obtained from FEA simulations were slightly higher than that from actual tests. The thicknesses of the beams used in FEA analysis were 1.40 mm and 1.54 mm for thinner and thicker beams respectively. The actual beam thicknesses for some of the conformal elements were higher as shown in Table 4.1. Due to the increased thickness, the elements were able to absorb more energy which resulted in lesser impact acceleration values during actual testing. As the beam thicknesses used in the simulation is lower, the force threshold is also lower. Due to this, the prediction for smaller impacts (for 3 and 6 inch drop heights) is also lower. The FEA analysis can be made more accurate by incorporating the varying thicknesses of the beams of the elements.

The material properties for the head form was also obtained from extrapolation which could also be a cause for the difference in results of FEA simulations and experimental tests.

4.4. SUMMARY

In this chapter, physical experiments were conducted to evaluate the impact performance characteristics of the conformal elements. The conformal elements were subjected to both quasi static testing and impact testing. The experimental procedure and the results were discussed in detail. The performance of the conformal elements was compared to that of conventional baseball foam padding, and the conformal elements outperformed conventional baseball foam padding for low as well as high impacts. The FEA predictions were compared with the experimental test data and found to be in close agreement with one another.

Chapter 5: Closure

5.1 SUMMARY

The focus of this research was to study the implementation of conformal negative stiffness elements for impact isolation in baseball helmets. The aim was to tailor the design of these conformal elements to the application and incorporate these modified conformal designs into a padding that could be used in baseball helmets and caps for providing better protection against impacts.

Chapter 1 started with establishing the need for a better impact absorbing element in baseball for batters and pitchers. Previous work regarding negative stiffness structures was also discussed. The research done by Qiu *et al.,* (2004) in the utilization of pre-curved beams for bi-stable mechanisms was discussed. It was followed by the adaptation and application of pre-curved beams to develop mono-stable structures and subsequent implementation to develop negative stiffness honeycomb structures [Kashdan *et al*., 2009, Schaedler *et al*., 2011, Fulcher *et al*., 2014, Correa *et al*., 2015]. The subsequent development of a conformal design by Debeau and Seepersad (2017) was also discussed. In this chapter, the aim and focus of the research was also established.

Chapter 2 described the negative stiffness honeycombs in greater detail. The basic equations and underlying principles governing the behavior of pre-curved beams were discussed. Conditions for mono-stability and bi-stability were also discussed. The conformal design was introduced, and the principles governing pre-curved beams in the context of conformal design were also explained. A conformal negative stiffness element was designed specifically for this application. However, there was a need to increase the effectiveness of these elements; hence, a novel concept of conformal elements having variable force thresholds was introduced. The methods to introduce variable force

threshold in the conformal design were discussed. Subsequently, conformal elements were designed with variable force threshold. Four sample specimens were additively manufactured in nylon 11 through SLS. Finally, a design of an impact isolating padding that integrates the conformal elements was presented.

The FEA of conformal elements was explained in Chapter 3 of this research. The conformal elements were subjected to both quasi-static and dynamic analysis using ABAQUS. The assembly of the model, analysis procedure, interactions and boundary conditions were explained in detail. Quasi-static simulation was conducted to predict the force threshold of the curved beams. FEA impact simulation was also conducted to correspond to a drop height of 12 inches, and the maximum impact acceleration experienced by the head form was simulated.

Chapter 4 of the research covered the physical testing that was performed on the conformal elements. All four samples were subjected to quasi-static testing, and their force thresholds were recorded. The elements were also subjected to impact testing from different drop heights. The performance of the conformal elements was compared to that of baseball foam. Finally, the conformal elements were placed inside of the helmet and subjected to impact testing from different drop heights. The results from physical testing were compared to those obtained from FEA and were found to be in agreement with each other.

The conformal elements outperformed conventional baseball foam padding in all of the impact tests – for a range of impact velocities. For smaller impacts, i.e. for drop height of 3 inches, the impact acceleration for conformal elements was in the range of 14 g to 17 g while that for baseball helmet foam was 18 g to 25 g. For 6 inch drop, the impact acceleration for conformal elements was thresholded at 20 g to 23 g, while for the foam it

was 35 g to 40 g. The conformal elements performed better for higher impacts as well. For drop height of 12 inches and 24 inches, the impact acceleration for conformal elements was measured in the range of 35 g to 40 g and 70 g to 75 g respectively, in comparison to the foam padding for which the corresponding impact acceleration was in the range of 57 g to 62 g and 90 g to 100 g respectively. This research demonstrates the potential of conformal negative stiffness elements as a shock absorbing element. The design of the conformal elements can be tailored to specific applications, as well. As was the aim of this research, conformal elements exhibiting better performance characteristics than conventional baseball foam padding were successfully designed and developed.

5.2 FUTURE WORK

More testing of conformal elements inside the helmet needs to be carried out with controlled impulse inputs to better characterize the performance of the conformal elements. Impact testing from different directions to simulate the effect of a baseball hitting the helmet would help in better performance evaluation of the conformal elements. Further, testing with a standard instrumented head form and neck form would provide more accurate performance evaluations that could be compared with other published studies. These instrumented head forms allow for accelerometers and sensors to be mounted on different positions of the head form and neck. The elements could also be tested under repeated impacts for fatigue performance evaluation. Efforts are underway to develop an instrumented drop test rig with a Humanetics head form. Accelerometers mounted inside the head form will provide more realistic impact mitigation data. The layered conformal negative stiffness design, one of the two concepts discussed to introduce variable threshold in the conformal elements, needs to be further investigated and compared to the standard

conformal design. There is scope for improvement in the design of the padding itself to make it more comfortable. Different materials and manufacturing approaches could also be tested to help reduce the overall dimensions of the conformal elements.

References

Viano, D. C., McCleary, J. D., Andrzejak, D. V., & Janda, D. H. (1993). Analysis and comparison of head impacts using baseballs of various hardness and a hybrid III dummy. *Clinical Journal of Sport Medicine*, *3*(4), 217-228.

Rutherford, G. W., Kennedy, J., & McGhee, L. (1984). Hazard analysis: baseball and softball related injuries to children 5-14 years of age. *US Consumer Product Safety Commission, Epidemiology, Division of Hazard Analysis*.

Gessel, L. M., Fields, S. K., Collins, C. L., Dick, R. W., & Comstock, R. D. (2007). Concussions among United States high school and collegiate athletes. *Journal of athletic training*, *42*(4), 495.

McCrea, M., Hammeke, T., Olsen, G., Leo, P., & Guskiewicz, K. (2004). Unreported concussion in high school football players: implications for prevention. *Clinical journal of sport medicine*, *14*(1), 13-17.

https://baseballsavant.mlb.com/statcast_leaderboard

Rowson, S., & Duma, S. M. (2011). Development of the STAR evaluation system for football helmets: integrating player head impact exposure and risk of concussion. *Annals of biomedical engineering*, *39*(8), 2130-2140.

Schaedler, T. A., Jacobsen, A. J., Torrents, A., Sorensen, A. E., Lian, J., Greer, J. R., & Carter, W. B. (2011). Ultralight metallic microlattices. *Science*, *334*(6058), 962-965.

Fulcher, B. A., Shahan, D. W., Haberman, M. R., Seepersad, C. C., & Wilson, P. S. (2014). Analytical and experimental investigation of buckled beams as negative stiffness elements for passive vibration and shock isolation systems. *Journal of Vibration and Acoustics*, *136*(3), 031009.

Kashdan, L. B., Haberman, M. R., Wilson, P. S., & Seepersad, C. C. (2009). Negative stiffness metamaterial elements for enhanced material damping capacity. *The Journal of the Acoustical Society of America*, *126*(4), 2280-2280.

Qiu, J., Lang, J. H., & Slocum, A. H. (2004). A curved-beam bistable mechanism. *Journal of microelectromechanical systems*, *13*(2), 137-146.

Klatt, T., Haberman, M., & Seepersad, C. (2013). Selective laser sintering of negative stiffness mesostructures for recoverable, nearly-ideal shock isolation. In *Proceedings of the solid freeform fabrication symposium. The University of Texas at Austin, Austin, TX*.

Correa, D. M., Klatt, T., Cortes, S., Haberman, M., Kovar, D., & Seepersad, C. (2015). Negative stiffness honeycombs for recoverable shock isolation. *Rapid Prototyping Journal*, *21*(2), 193-200.

Debeau, D. A., & Seepersad, C. C. (2017) Additively manufactured conformal negative stiffness honeycombs. In *Proceedings of the solid freeform fabrication symposium. The University of Texas at Austin, Austin, TX.*

Debeau, D. A., Seepersad, C. C., & Haberman, M. R. (2018). Impact behavior of negative stiffness honeycomb materials. *Journal of Materials Research*, *33*(3), 290-299.

https://www.nist.gov/sites/default/files/documents/el/isd/Plenary_Stucker.pdf

Fernandez-Vicente, M., Calle, W., Ferrandiz, S., & Conejero, A. (2016). Effect of infill parameters on tensile mechanical behavior in desktop 3D printing. *3D printing and additive manufacturing*, *3*(3), 183-192.